Pro Gradu

Quantum Size Effect in Low Dimensional Bismuth Nanostructures.

Kari-Pekka Riikonen
8.4.2009

University of Jyväskylä
Department of Physics
Nanoscience Center

Tiivistelmä suomeksi

Työn nimen voisi suomentaa ”Koosta riippuvainen kvantti-ilmiö dimensioiltaan rajoitetuissa vismuttisissa nanorakenteissa”. Työssä pyrittiin havaitsemaan vapaaelektronitilojen muutoksien vaikutusta sähkönjohtavuuteen pienissä vismuttirakenteissa, joiden kokoa voitiin kutistaa ionisuihkumenetelmällä, eli niin kutsutulla sputteroinnilla.

Jos johtavan aineen jokin dimensio voidaan kutistaa niin pieneksi, että se on verrannollien ko. johteen vapaiden varaustenkuljettajien aineaallonpituuteen, on kyseessä sähköisten ominaisuuksien kannalta alhaisten dimensioiden rakenne. Toisin kuin makroskooppisessa, klassisen sähköopin lainalaisuuksia noudattavassa johteessa, nanoskooppisesssa rakenteessa itse rakenteen muoto ja koko voivat vaikuttaa rakenteen sähköisiin ominaisuuksiin. Tämä johtuu vapaiden elektronien energiatilojen kvantittumisesta rakenteen koon lähestyessä vapaiden elektronien aineaallonpituutta. Ilmiön havaitsemisen kannalta ihanteellisella materiaalilla on alhainen Fermienergia ja pieni vapaiden elektronien efektiivinen massa, sekä näistä ominaisuuksista johtuen - alhainen varaustiheys. Vismutti osoittautuu tässä suhteessa ihanteelliseksi näytteiden valmistusmateriaaliksi, koska sillä on verraten alhainen Fermienergia 38 meV ja sen vapaiden elektronien efektiivinen massa on pienimmillään jopa tuhannesosa elektronin normaalista massasta. Efektiivisellä massalla tarkoitetaan johteiden yhteydessä sitä, että aineessa olevat johtavuuselektronit käyttäytyvät ikään kuin niiden massa poikkeaisi normaalista vapaan elektronin massasta. Pieni efektiivinen massa tarkoittaa mm. sitä, että tiettyä energiaa vastaava elektronin aineaallonpituus eli ns. de Broglien aallonpituus on tällaiselle elektronille suurempi. Ominaisuuksistaan johtuen joidenkin johtavuuselektronien aallonpituus fermienergialla vismutissa on jopa 100 nm. Tämä tarkoittaa, että johtavuuselektronien energiaspektri tulee diskreetiksi jo, kun rakenteen jokin dimensio saadaan kutistettua satojen nanometrien kertaluokkaan. Useimmilla muilla metalleilla, joille fermienergia on elektronivolttien luokkaa ja johtavuusleketronien efektiivinen massa lähellä elektronin massaa tyhjiössä, johteen elektronitilojen energioiden diskreetti luonne tulisi esille vasta muutamien nanometrien kokoluokassa. Vismutin tapauksessa johtavuuselektronien aallonpituus on kuitenkin niin

suuri, että ilmiötä on mahdollista tutkia näytteillä, jotka on valmistettu elektroniikkateollisuudesta tutulla litografiamenetelmällä. Menetelmällä pystytään helposti valmistamaan metallisia näytteitä, joiden dimensiot ovat satojen nanometrien luokkaa. Lisäksi tämän kokoluokan näytteitä voidaan edelleen hallitusti kutistaa pienemmiksi ionisuihkulla sputteroimalla. Muutaman nanometrin kokoluokassa tämä ei olisi mahdollista koska aineen atomaarinen rakenne tulisi oleellisesti rajoittavaksi tekijäksi. Lisäksi vismutille on ominaista, että se muodostaa helposti suurikiteisiä rakenteita. Tämäkin on hyödyllinen ominaisuus sikäli, että kiderajat vaikuttavat energiatiloihin muodostamalla kiteiden väliin elektronien kannalta potentiaalivalleja.

Työssä oli tavoitteena valmistaa vismutista ohuita, efektiivisesti kaksiulotteisia nanofilmejä ja efektiivisesti yksiulotteisia nanolankoja, joita edelleen kulutettiin pienemmiksi ionisuihkumenetelmällä. Näytteiden sähkönjohtavuutta mitattiin askeleittain pienenevien dimensioiden funktiona. Yksi mittaussykli sisälsi näytteen jäähdytyksen kryogeeniseen lämpötilaan, sähköisen vastustuksen mittaamisen nelipistemenetelmällä, lämmityksen takaisin huoneen lämpötilaan ja sputteroinnin ionisuihkulla. Mittaus-sputterointisyklejä jatkettiin tyypillisesti niin kauan kuin näyte säilyi ehjänä. Odotuksena oli, että näytteiden johtavuus ei laske monotonisesti, vaan sillä on paikallisia maksimeita sellaisilla filmin paksuuden tai langan halkaisijan arvoilla, joilla jokin sen johtavuuselektronien tiloista saavuttaa fermienergian, jolloin varaustiheys ja varauksenkuljettajien liikkuvuus on maksimissaan. Halkaisijan muilla arvoilla elektronien energiat halkaisijan suunnassa ovat selvästi pienempiä. Teoreettisesti on laskettu, että tällaisen oskillaation periodi olisi 50 nm, tietyssä kideakselin suunnassa. Aikaisemmissa tutkimuksissa on menestyksellisesti tutkittu kokoriippuvuuden vaikusta Hall-ilmiöön vismutissa. Em. tutkimuksissa on käytetty erillisiä eri paksuisia efektiivisesti kaksiulotteisia näytteitä. Tässä työssä oli tarkoitus tutkia sähkönjohtavuuden muutoksia samassa näytteessä, kun sen kokoa kutistettiin ja erityisesti ohuissa, ihanteellisesti monokristallisissa lankanäytteissä, joissa kokoriippuvien ilmiöiden todentaminen on osoittautunut hankalammaksi.

Työssä onnistuttiin havaitsemaan epämonotonista sähkönvastuksen kasvua kutistuvien dimensioiden suhteen sekä filmi että lankanäytteissä. Havaitun oskillaation periodi ja amplitudi eivät tosin vastanneet teoreettisia odotusarvoja, mutta on syytä

kuitenkin olettaa, että havaittu oskillaatio liittyy johtavuuselektronien energiatilojen kvantittumiseen. Teorian ennustamien ja mitattujen ominaisuuksien ilmeinen ristiriita selittynee sillä, että teoria olettaa näytteellä olevan monokristallisen rakenteen ja näytteen tietyn kideakselin suuntaisen orientaation kutistettavien dimensioiden suuntaan nähden. Todellisuudessa ohuet lankanäytteetkin koostuivat useammasta yksittäisestä kiteestä ja niiden kideakselien orientaatio näytteen akselin suhteen vaihteli. Vismutin johtavuuselektronien efektiivinen massa riippuu oleellisesti tarkastelusuunnasta, ja havaittu, verraten satunainen oskillaatio voi selittyä sillä, että eri kiteiden osuus sähkönjohtavuuteen oli erilainen.

In memory of my father

Contents:

Tiivistelmä suomeksi II
1 Introduction 1
2 Theory 4
2.1 A quantum particle in a potential well 4
2.2 Origin of the size quantization of energy in a metal lattice 7
2.3 Requirements of observing quantum size effects in 2D and 1D limits 10
2.4 Band structure of Bismuth 13
2.5 Advanced models 16
3 Existing studies on QSE 20
4 Methodology 23
4.1 Sample fabrication and preparation 23
4.2 Fabrication and structural analysis of film samples 30
4.3 Measuring setup 31
4.4 Sputtering setup 33
5 Results and discussion 35
5.1 Sputtering 35
5.2 QSE Measurements 44
5.2.1 QSE measurements of the film samples 46
5.2.2 QSE measurements of the wire samples 49
6 Conclusions 59
Acknowledgments 60
References 61
List of publications contributed by author 63

.

1 Introduction

Quantum particles in a potential well can only have such energy levels which give the particles a wavelength which fits an integer number of times in the well. The lowest energy state corresponds to a wavelength which is two times the size of the well, the second lowest state corresponds to a wavelength which is the size of the well etc. Generally allowed wavelengths are $\lambda = 2L/n$ where λ is the de Broglie wavelength, L is the length of the well and n is an integer. If the wavelength of the particles is comparable to the size of the well, then the energy spectrum of the system becomes essentially discrete. If the corresponding particles are fermions, which quantum states are restricted by the Pauli exclusion principle, then only two particles can occupy the same energy state.

Size phenomena in solids come into play when the dimensions of a system are comparable to the characteristic scale of the corresponding physical process. If the process can be adequately described in classical terms (e.g. electric resistivity in metals) with the mean free path setting the scale, then the corresponding phenomena are called classical size effect. Quantum size effect (QSE) should be considered if the dimensions of the system are comparable to the de Broglie wavelength of the particles (e.g. conducting electrons in a metal). Then the size of the system determines the allowed energy levels.

QSE in metals originates from the discrete electron energy levels in very small metal structures which acts as potential well for the electrons. If dimensions of the sample are of the order of the wavelength of electrons in the metal, and if the concentration of electrons is low then the energy spectrum of electrons is essentially discrete. By changing

the dimensions of the structure the concentration of the conducting electrons can be altered, which in turn will affect the conductivity of the sample in a non-classical manner. If the dimensions of the sample could be varied its conductivity should have local maxima at points where a certain electron energy state reaches the Fermi level. This effect happens when some of the dimensions of the sample equal a multitude of one half of the wavelength of the electrons at Fermi energy in that particular metal, for then the concentration and mobility of the electrons is highest.

Bismuth is exceptionally good material for observing the QSE as it has low Fermi energy and its electrons have a small effective mass. Therefore electrons near the Fermi level have very long wavelength, even 100 nm in some directions. This is in the scale range of lithographical manufacturing methods and workable sputtering operation.

Study of quantum size effect in low dimensional bismuth structures started already in the 1960's. Basic theories and the manufacturing principles of suitable samples were largely developed in former Soviet Union and the foundation of the whole area of research was laid down at the time. Nowadays the most notable contributor on the field is arguably Prof. M. S. Dressehaus and her research group at MIT, who have made many experiments on the subject.

In this thesis bismuth nanowire and film structures were studied. Wire samples were made by e-beam lithography on mica substrate, film samples were evaporated through a mechanical mask. Samples were analyzed with AMF. From AFM images the individual crystals could be distinguished and suitable samples could be chosen for measurements. Especially the objective was to produce a single crystal wire sample, but later the requirements had to be lowered as it turned out to be very difficult to produce such samples. I(V) measurements were made with AC and DC modes at room temperature, as well as at liquid nitrogen and helium temperatures. Between the measurements the samples were reduced in size by ion beam sputtering, which was used to consume the surface of the sample from few atomic layers to tens of nanometers during a single sputtering session. Measurement-sputtering cycles were continued as long as the sample survived. Typically at some stage the sample was destroyed.

The results of the thesis are of significant importance for the basic science demonstrating existence of the fundamental quantum phenomenon – quantum size effect.

In this work the sputtering was used as a fabrication tool to reduce the size of the sample, but it is also interesting itself as a surface treatment method which may have a broad field of applications in industry and research.

2 Theory

2.1 A quantum particle in a potential well

A quantum particle in a potential well is a classical problem that is introduced to all physics students when they start studying modern physics and quantum mechanics. The problem is typically simplified by assuming the well is a square potential and infinitely deep. This idealization makes the problem much easier to handle and in many cases it describes the real system well enough.

According to the principles of quantum mechanics, a quantum particle could be considered as a wave with a wavelength λ. This wavelength is called the de Broglie wavelength and it is defined as:

$$\lambda = \frac{h}{p} \qquad (1)$$

Where h is the Planck's constant and p is the momentum of a particle. Wave number k is defined by the wavelength as:

$$k = \frac{2\pi}{\lambda} \qquad (2)$$

According to classical mechanics the energy of a particle can by expressed by its momentum and by its mass as:

$$E = \frac{p^2}{2m} \tag{3}$$

When we sum up the equations 1-3 and remember that $\hbar = h/2\pi$, we can determine the quantum mechanical energy of a moving particle by the wave number, which is:

$$E = \frac{\hbar^2 k^2}{2m} \tag{4}$$

Wave function of a free particle which is moving in direction x is of the form:

$$\psi(k) = Ae^{ikx} \tag{5}$$

If a particle is restricted to an infinite square potential well with length d where the bottom of the well is at zero potential all the way between the barriers, and if the potential is time independent, the wave function reduces to simpler form and is given by:

$$\psi(x) = \sqrt{\frac{2}{d}} \sin\left(\frac{n\pi x}{d}\right) \tag{6}$$

Here the wave number k is now replaced with $\frac{n\pi}{d}$, where n is an integer and marks the number of complete 2π waves that fit inside the well, and k can therefore only get discrete values corresponding to a certain n. When we substitute k in Eq. (4) with $\frac{n\pi}{d}$, we'll see that the energies of such a particle are also discrete with allowed values of

$$E_n = \frac{\hbar^2 \pi^2}{2d^2 m} n^2 \tag{7}$$

For a free particle in three dimensions the general form of wave function is

$$\psi(\vec{k}) = Ae^{ikx} e^{jky} e^{lkz} \tag{8}$$

In Eq. (8) parts of the wave function corresponding to different spatial coordinates can be separated. If now the movement of the particle is restricted in one dimension, say in *x*, to a very narrow region, we can replace the general exponential form with sinusoidal one from Eq. (6). That is, if direction *x* is limited to a dimension *d* which is compared to the wave length of that particle. In such a case we may write the wave function as:

$$\psi(\vec{k}) = \sqrt{\frac{2}{dL_y L_Z}} \sin\left(\frac{n_x \pi x}{d}\right) e^{jky} e^{lkz} \tag{9}$$

In practice this could describe for example an electron in a thin metal film with thickness *d* and length L_y and width L_z. For a thin wire, or a nanowire, with limited thickness and width and with large length, the wave function would be

$$\psi(\vec{k}) = \sqrt{\frac{2}{dwL}} \sin\left(\frac{n_x \pi x}{d}\right) \sin\left(\frac{n_y \pi y}{w}\right) e^{lkz} \tag{10}$$

[1] In which *d*, w and *L* are thickness, width and length of the quasi-one-dimensional sample respectively.

2.2 Origin of the size quantization of energy in a metal lattice

Electrons in metal can be described to some extent by the ideal model of a quantum particle in a potential well, as they are confined in the metal and have a very small probability of escaping the well at mild temperatures. It requires that the 'well' of a metal sample is smaller than the mean free path of electrons, and that it is a single crystalline structure, so that the scattering of electrons happens only at the boundaries. This simplified model works especially at very low temperatures at which the mean free path of electrons is longer due to less phonon interactions.

Electrons are fermions whose quantum states are restricted by Pauli exclusion principle. It states that several fermions can not exist on the exactly same quantum state in the same region of space. It means that only two electrons with opposite spins can occupy the same energy level at the same moment in time. Therefore if there are several electrons in the well, they must occupy higher and higher energy states, even at close to zero temperature. Energies of the different states are given by the Eq. (7)

One definition of Fermi energy for metals is that, it is the highest energy of any free electron in that metal at absolute zero temperature. When temperature rises, thermal fluctuations of electron energies cause some electrons near the Fermi level to be exited to higher states above the Fermi level. Probability P of an energy state with energy E to be occupied in an uncharged piece of metal with Fermi energy E_F is:

$$P(E) = \frac{1}{\exp\left(\frac{E - E_F}{k_B T}\right) + 1} \qquad (11)$$

As the thermal energy of a particle is of the order of $k_B T$ and the Fermi energy in typical metals is of the order of electron volts, it is obvious that only electrons near the Fermi level may transfer from one energy level to another, since there are free energy states only above the Fermi level. States far below the Fermi level are occupied, and they are

therefore not largely affected by thermal excitations. Schematic plot of Fermi distribution function Eq. (11) at a finite temperature is presented in Fig. 2.1. It should be emphasized that the picture is figurative and thermal broadening of the energy distribution is exaggerated for visual reasons. For example, the Fermi energy of copper is 7.0 eV while broadening $k_B T$ at room temperature would be only ~25 meV.

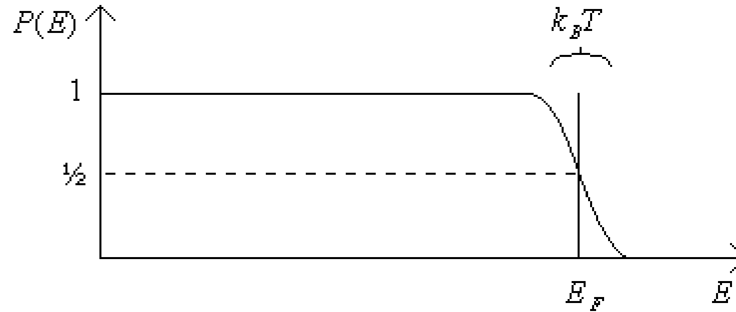

Fig. 2.1: *Schematic plot of Fermi-Dirac distribution. A probability of an energy state with energy E in metal to be occupied.*

Another definition for Fermi energy is that it is the energy level that is occupied by a probability of ½ at a mild temperature. At low temperatures this and the earlier definition give practically the same energy value for the Fermi energy. This latter definition comes from the self-evident fact, that as electrons are excited from an energy level below Fermi level to some level above it, then somewhere in between there is the level at which the occupation number is ½. And as the thermal broadening of the step in the distribution is very narrow compared to Fermi energy, the energy state with the occupation number of ½ is very close to Fermi level.

Fermi distribution is a very steep step function which practically has a value of one for $E < E_F$ and it vanishes quickly to zero with energies higher than Fermi energy. Especially at very low temperatures. Increase in temperature makes the step shallower as seen in Fig. 2.1. Since electron energies are practically limited to the Fermi energy, their wave number vector is also limited to a corresponding value of k_F, which forms a surface in reciprocal *k*-space. All states corresponding to a *k*-vector that fit inside this

Fermi surface are occupied and almost all other states are empty. Spherical Fermi surface in *k*-space is represented in Fig. 2.2 (a). If we have a two dimensional electron gas, which has a thickness comparable to the de Broglie wavelength of electrons, then, according to Eq. (7), the energy spectrum becomes discrete in that restricted direction, while being continuous in others. Allowed states inside the Fermi sphere will then be planar disks. Such states in *k*-space will take the shape represented in Fig. 2.2 (b). If dimensions of electron gas are limited in two directions to quasi-one-dimensional limit, the energy spectrum will become discrete in both directions. Fig. 2.2 (c) represents such situation. Allowed *k*-vector values are restricted in *z*-direction to lateral planes and in *y*-direction to vertical ones. So all in all, allowable *k*-vectors are positioned at the cross sections of lateral and vertical planes and they form thin lines stretching from one side of the initial Fermi sphere to another.

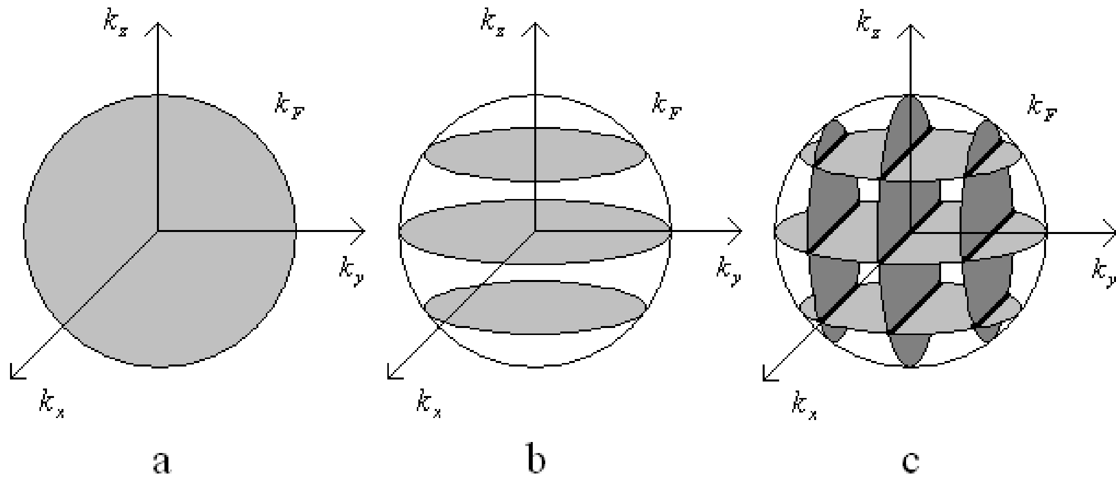

Fig. 2.2: *(a) represents continuous free electron states in k-space for a three dimensional bulk sample, (b) allowed states of an electron gas that is limited in z-direction to quasi-two-dimensional and (c) represents an electron gas that is restricted in z- and y-directions, or which is quasi-one-dimensional. Allowed k-vectors are located at cross sections of vertical and horizontal discs.*

Allowed energy levels of electrons in a metal are thermally broadened by a factor which is comparable to $k_B T$. If two states are separated by an energy gap smaller than

$k_B T$ they overlap each other and the energy spectrum between them is continuous. By cooling down the metal, energy levels became 'thinner' and if centers of the energy levels are far enough from each other the overlapping vanishes and energy levels are separated. In Eq. (7) we can see, that if dimension d of the sample is reduced, the energy gap between two states, E_n and E_{n+1}, grows. Requirement for energy to become quantized is that energy levels of two adjacent states must be separated by an energy gap which is larger than the thermal energy, so that the condition $E_{n+1} - E_n > k_B T$ holds.

For real electrons in a metal lattice, the Fermi surface is generally not a perfect sphere. In lattice some directions of movement for electrons may be more favorable than others. That has been taken into account by considering electrons to have an 'effective mass' which differs from the real electron's mass m_0 and is different in different directions of movement. In addition, in metals the *k*-vectors of conducting electrons must fit inside the 1st Brillouin zone of the reciprocal lattice. Larger *k*-vector values correspond to wavelengths that are smaller than the lattice constant and such electrons will quickly lose their energy in scatterings with the lattice. Still the size effect for the quantization of energy levels is similar in quality to the one expressed in Fig 2.2.

2.3 Requirements of observing quantum size effects in 2D and 1D limits

If one wants to observe the size effects related to quantized energy states in a metal, then at least one of the dimensions must be of the order of the de Broglie wavelength of electrons in that metal. If the dimensions of the sample are larger, the spacing between quantized energy levels is small and they will overlap because of the thermal broadening of the states. So the crucial requirement for the energy levels close to Fermi energy is that $E_{n+1} - E_n > k_B T$. In theory this condition could always be met by making the samples small enough, but practical limitations of sample manufacturing rule out the use of most metals. Estimations show that for metals with high concentration of electrons like Au, Cu or Al the Fermi energy is of the order of electron volts and as effective masses of their

electrons are large $m^* \approx m_0$, it requires diameters of $d \sim 1$ nm from the sample to satisfy the above condition as can be seen from Eq. (7). A 'good' candidate should have a low Fermi energy and a small effective mass of its electrons, so that its de Broglie wavelength at Fermi energy would be as long as possible. The sample's dimensions must also be smaller than the mean free path l of electrons in a bulk metal, so that scattering would happen mostly on the walls of a sample and not inside the volume. So $l \geq d$ must hold [2]. This also means that the sample must be made of as pure material as possible, since impurities increase scattering. Further more, it is beneficial if the chosen metal is such that it is easy to fabricate large uniform crystal samples from it, as crystal boundaries and defects also cause electron scattering. The surface roughness must be small compared to the wavelength of electrons. And finally, observation must be done at low temperatures, as it reduces the energy level broadening and so helps to resolve the quantized energy spectrum.

When dimensions of the sample are reduced, the energy levels move upwards in energy and as they pass the Fermi level one by one, the density of states near the Fermi level oscillates between higher and lower values. Since the electrons close to the Fermi level are mostly responsible for electric conductance in metals, the variation in density of states causes the resistance to change non-monotonously relative to the size of the sample. Meaning, that if the resistance of an effectively one dimensional sample is measured as a function of the decreasing cross section of the sample, the resistance would show oscillatory behavior. Ultimately the sample should turn into a semiconductor, as the last free electron states pass the Fermi level and an energy gap is formed between conduction and valence bands. That includes an assumption that the Fermi level itself is relatively stable compared to the energy level spacing of the electron states, so that it is not largely affected by the dimensional variation. This is an important aspect since Fermi energy does not have by default any fixed value, but is determined by the energy spectrum. As energy levels themselves are changing as function of the dimensions, one should be aware of the possibility the Fermi energy may be affected as well. Fig. 2.3 is a schematic picture of the electron states in a metal whose effective mass of holes is much greater than that of its free electrons. As the metal is overall electrically neutral, there must be an equal number of holes, or unoccupied electron states of the valence band above the Fermi

level and occupied free electron states under it. Density of states in energy for holes is much greater than for electrons, since that is proportional to the mass of the particle. It can be seen in Eq. (7), that energy level spacing of two adjacent levels is proportional to the effective mass of the particles; $E_{n+1} - E_n \propto 1/m^*$. For this reason the energy range covered by holes from Fermi level to the top of the valence band is much smaller than energy range covered by free electrons, which in turn is measured from the bottom of the conduction band up to the Fermi level. If dimensions are reduced, the electron states move upwards in energy as electron wavelength is forced to decrease by the change in dimensions, hole states are not affected that much as holes are heavier and have smaller de Broglie wavelengths. The Fermi level is always under the top of the valence band in energy, as long as there is band overlap at all. The Fermi level is therefore relatively stable and close to the top of the valence band in a material in which the effective mass of holes is much greater than the effective mass of electrons, and it is not affected much by the varying dimensions.

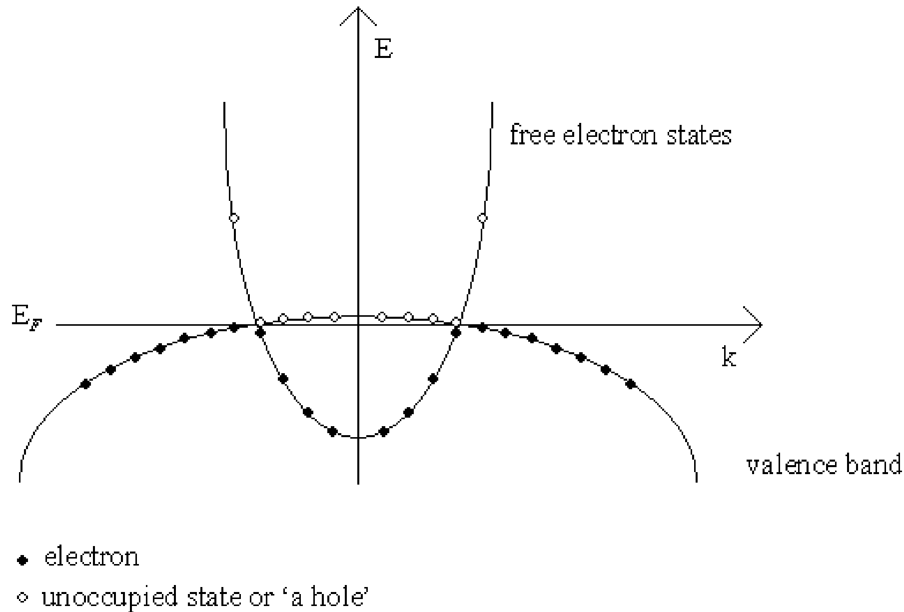

Fig. 2.3: *Electrons prefer to occupy lowest energy states up to the Fermi energy, whether the state is a valence state or a free electron state. This leaves unoccupied states in the valence band, which can act as positive charge carriers with negative masses.*

It turns out, that bismuth fulfills well all the requirements of an ideal material to observe QSE in metals. Bismuth has a low Fermi energy $E_F \approx 30$ meV and it is technologically possible to achieve an energy level spacing of ~10 meV, while at liquid helium temperature the thermal broadening is much smaller $k_B T \approx 0.4$ meV [3]. In bulk samples one can obtain the mean free path $l \approx 1$ mm at 4.2 K. [4]. It has a relatively stabile Fermi energy due to its relatively large difference in effective masses of its free electrons and heavy holes. And in addition, it is also easy to produce large ($d \sim 1$ μm) and smooth surfaced crystals from it with lithographical methods.

2.4 Band structure of Bismuth

Bismuth crystal lattice has a rhombohedral unit cell with lattice constant a = 454.950 pm, that is basically a simple cubic cell which is stretched along its diagonal axis so that the length of the diagonal c is 1186.225 pm [22]. Schematic picture of a rhombohedral unit cell is shown on the left side in Fig. 2.4. In bismuth the lattice vectors marked with letter a are at 30˚ angle relative to the diagonal axis which is marked with letter c, diagonal axis is also called the trigonal axis. Lattices with rhombohedral unit cells form a hexagonal crystal structure as shown on the right side of Fig. 2.4. Rhombohedral crystal structure has a hexagonal shape, when viewed from the angle of the trigonal axis.

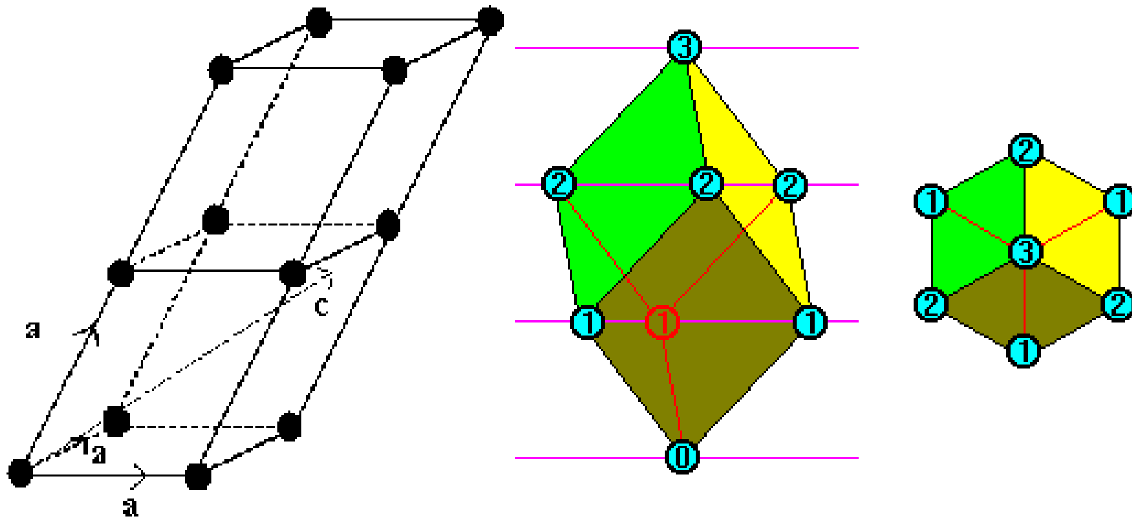

Fig. 2.4: *On the left semantic picture of rhombohedral crystal structure, on the right rhombohedral-hexagonal transformation.*

On the left in Fig. 2.5 there is a 1st Brillouin zone of the bismuth lattice where points of conductive electron pockets are marked with *L* and a single hole pocket with *T*. Those pockets are regions of the previously discussed Fermi volume that fit inside the 1st Brillouin zone. As mentioned before, the Fermi volume in metals is generally not a perfect sphere. In case of bismuth the *k*-vectors of conductive charge carriers are limited to a few separate pockets, but still the energy levels in side those pockets become similarly discrete in certain directions as in the case of free electron gas, when the dimensions of the sample are reduced. Lattice stress may also affect the lattice constant in some directions and can change the shape of the Brillouin zone and pockets of the free charge carriers in it.

Effective mass tensor for the charge carriers in bismuth is presented on the right side of Fig. 2.5. For electrons the effective masses are very small, in some directions they are almost one thousand times smaller than the free electron mass m_0, while holes are generally much heavier. Effective masses of all charge carriers vary quite a lot depending on the direction of movement. From the energy quantization point of view this means that energy level spacing of charge carriers depends highly on direction in which electronic properties are studied. This is an important aspect if one tries to measure properties of

polycrystalline structures, since crystals may have different orientations and therefore contribute differently to the property that is measured.

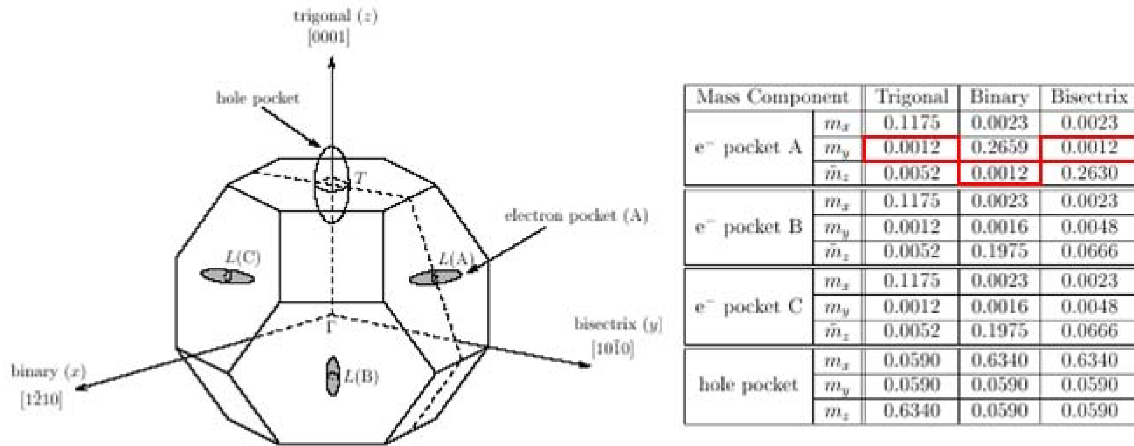

Mass Component		Trigonal	Binary	Bisectrix
e^- pocket A	m_x	0.1175	0.0023	0.0023
	m_y	0.0012	0.2659	0.0012
	$\tilde{m}_z$	0.0052	0.0012	0.2630
e^- pocket B	m_x	0.1175	0.0023	0.0023
	m_y	0.0012	0.0016	0.0048
	$\tilde{m}_z$	0.0052	0.1975	0.0666
e^- pocket C	m_x	0.1175	0.0023	0.0023
	m_y	0.0012	0.0016	0.0048
	$\tilde{m}_z$	0.0052	0.1975	0.0666
hole pocket	m_x	0.0590	0.6340	0.6340
	m_y	0.0590	0.0590	0.0590
	m_z	0.6340	0.0590	0.0590

Fig. 2.5: *On the left the 1st Brillouin zone of bismuth with free electron pockets and one hole pocket, on the right the effective mass tensor for electrons and holes [9]. In some directions the electrons have a very small effective mass (a few of them emphasized by red rectangles).*

Fig. 2.6 shows plots of measured energy bands of bismuth. Letters under the diagram correspond to different points in the 1st Brillouin zone shown in Fig 2.5. Conducting charge carriers are located at *L* and *T* points where energy bands cross the Fermi level. In other areas the energies of the bands do not reach the Fermi level and carrier states corresponding to those *k*-vectors cannot therefore contribute to conductivity. Formally, if the temperature of the metal is risen more bands should contribute to the electric conductivity due to the broadening of the energy levels. However, in practice this should happen at such a high temperature that other contributors like lattice vibrations may degrade the electric conductivity.

Fig. 2.6: *Charge carrier energy levels of bismuth [5].*

2.5 Advanced models

Energy of charge carriers in mild temperatures must be somewhere between the bottom of the conduction band and the top of the valence band. In schematic picture Fig. 2.7 the overlapping of the energy bands is marked with Δ. In between there is the Fermi energy marked with E_F. Energy range for free electrons is marked with μ_e. Holes of the valence band occupy energy states from the top of the valence band down to the Fermi energy, marked with μ_h, and the total overlap in energy is $\Delta = \mu_e + \mu_h$.

Fig. 2.7: *Overlapping of energy bands decreases when the dimensions of the sample are reduced.*

For bulk bismuth the overlapping of valence and conduction bands is 38 meV [6]. As mentioned earlier, the widths of μ_e and μ_h are proportional to the effective mass of the charge carriers whose energy range they represent. That is because there must be an equal number of both positive and negative charges and because the density of states in energy is proportional to the mass of the particle. In bismuth for example the heaviest holes have effective masses 600 times larger than the effective mass of the lightest electrons, it means that μ_e must be much larger in energy than μ_h and therefore:

$$\mu_e = \Delta \frac{m^h}{m^h + m^e} \approx \Delta \qquad (12)$$

By solving the d from Eq. (7) for $n = 1$ and by replacing the E in it with μ_e, or with the μ_h for that matter, we get the minimum size d_0 for the conductor that can still have free charge carriers.

$$d_0 = \frac{\hbar \pi}{\sqrt{2M\Delta}} \qquad (13)$$

Where M is the reduced mass of charge carriers:

$$M = \frac{m^h m^e}{m^h + m^e} \qquad (14)$$

When the dimensions of the sample are reduced the bottom of the conduction band moves upwards while the top of the valence band goes down in energy. If ε_e and ε_h are shifts of the conduction and valence bands as marked in Fig. 2.7, it must hold that $\varepsilon_e / \mu_e = \varepsilon_h / \mu_h$ [7], because of the requirement of electric neutrality. If dimensions of the sample are reduced the overlap energy decreases and is $\Delta - \varepsilon_e - \varepsilon_h$. When dimension of the sample are reduced enough the overlap will disappear completely and an energy gap

is formed between the top of the valence band and bottom of the conduction band. The band gap is:

$$E_g = \Delta\left(\frac{d_0}{d}\right)^2 - \Delta \tag{15}$$

with positive values corresponding to a situation where band gap exists and negative values ($d > d_0$) to a situation of overlapping bands. For a two dimensional case the overlaps in different directions may be interpreted as components of the total band overlap energy so that $\Delta = \Delta_x + \Delta_y$ and the energy gap would then be

$$E_g = \Delta_x\left(\frac{w_o}{w}\right)^2 + \Delta_y\left(\frac{d_0}{d}\right)^2 - \Delta \tag{16}$$

for a sample of width *w* and thickness *d* [1].

Oscillation periods of electric properties due to the size quantization is expected to be d_0. So when the size is changed, every time when $d = d_0 n$, where *n* is an integer, density of states with energies close to Fermi energy, should rise. This could be understood so that when *d* reaches $d_0 n$ there is just enough space for an electron with the Fermi wave length. If the size is then decreased that very state *n* goes over the Fermi energy level and becomes unoccupied, while other available states are low in energy and the next level would not reach the Fermi energy until $d = d_0(n-1)$ and the density of states near the Fermi level gets high again. It also indicates that electric properties are not only affected by the number of available states, but the energy also affects the mobility of charge carriers and the thermo electric power (Seebeck coefficient) [8]. All these effects are of course remarkable only for very small *n*, that is, in small samples.

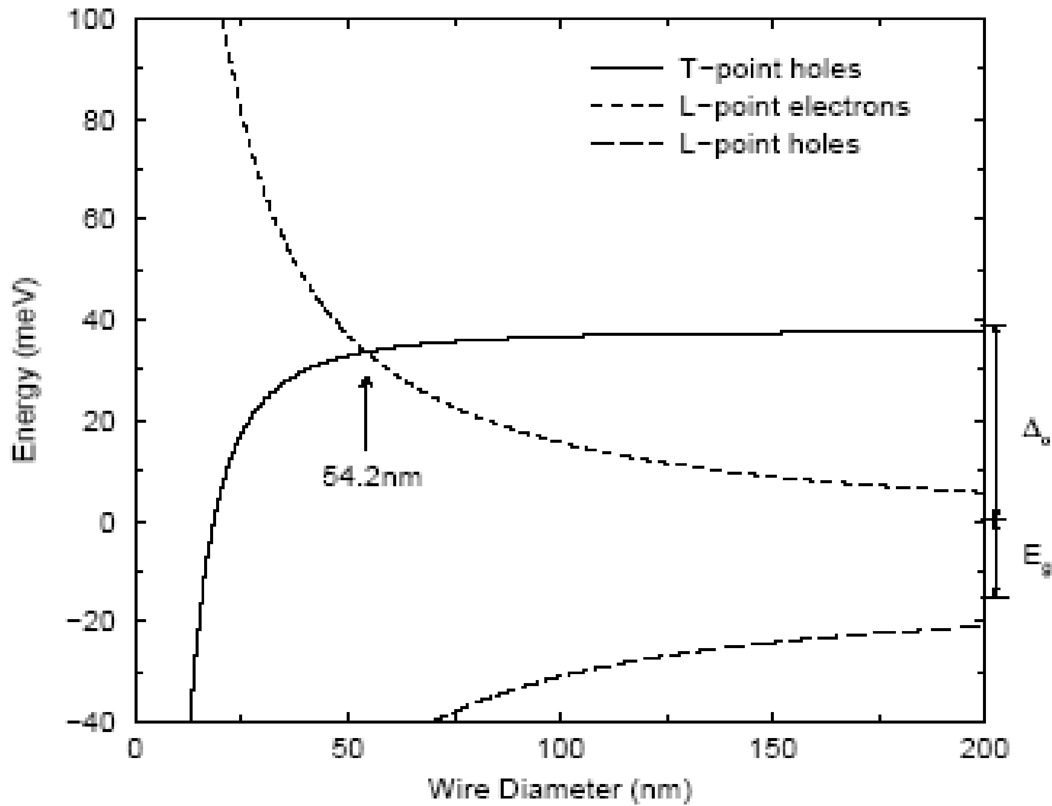

Fig. 2.8*: Theoretical calculations for energies of hole and free electron states as a function of the wire diameter, for a single crystal square cross sectional bismuth nanowire, with the trigonal axis along the wire and at 77 K temperature [9]. Metal to semiconductor transition should happen when the diameter reaches 54.2 nm.*

Stephen Cronin has calculated in his thesis [9] that a bismuth nanowire which is aligned along its trigonal axis and has a square cross section, should undergo the metal-semiconductor transition when the width and thickness exceed 54.2 nm. Energies for holes and electrons as function of thickness are plotted in Fig. 2.8. According to Cronin, the critical diameter should be 39.8 nm for a wire with binary crystalline orientation along the wire and 48.5 nm for a wire which is aligned along its bisectrix axis.

3 Existing studies on QSE

In many studies about the quantum size effect in bismuth, the approach to the problem has been that the properties of different sized films and nanowires have been studied with separate samples of different thicknesses. Main difference to my methodology was that I used the same sample which was then reduced in size by sputtering it with an ion beam. Nevertheless, several studies have shown evidence, that the electric properties of bismuth film oscillate as a function of the thickness with a periodicity of some tens of nanometers, when the thickness of the film is 100–300 nm, and when the crystals are mainly orientated on to their trigonal axis along the substrate normal [10, 4, 2 and 8]. This oscillation period is expected to correspond to one half of the wavelength of the free electrons in bismuth at Fermi energy in that direction. Theoretical calculations show that the oscillation period should be ~50 nm [3 and 9]. Theory also suggests that the corresponding 1D sample would ultimately undergo a metal-to-semiconductor transition when the sample is reduced to a smaller dimension than one half of that free electron's Fermi wavelength [1, 6 and 7].

In most of the studies where different thickness samples were distinct, the oscillation amplitude of the resistance at liquid helium temperature was measured to be some tens of percents of the total resistance. In Ref. [3] where a single sample was reduced in size by sputtering, the observed oscillation amplitudes were only a few percent of the total resistance at most. That is close to what I observed in my measurements and which were carried out in a similar fashion. In Ref. [10] it was found that the oscillation amplitude was damped when the film thickness decreased to less than 100 nm and that

oscillations turned beat-like instead of having a smooth sinusoidal form. A decrease of the period was also observed. In the paper these effects were speculated to be caused by the surface states and differently orientated crystals in the film. In Ref. [4] it was observed that the oscillation period was varying from 25 nm to 45 nm depending on the condensation conditions and the temperature of the substrate during evaporation. It was also found in the same study that the period depends on the film thickness and it was 10-15 nm when the film thickness was 80-140 nm and 25 nm periodicity was observed for films in the thickness range of 140-180 nm. In Ref. [2] and [4] a very similar oscillation of the resistance relative to the film thickness was measured, both having measured the maxima of the resistances to be located roughly at 110, 160 and 210 nm points of the film thickness.

In addition to the electric conductivity, other electric properties have been studied and are expected to show similar periodicity as a function of the film thickness. Some of the most studied subjects are Hall coefficient and magnetoresistance [1, 7 and 8]. In ref. [4] optical effects were studied by observing the light absorption coefficient of thin bismuth films. It was found that red absorption edge of photons increased from 0.07 eV for 300 nm thick film to 0.14 eV when the film thickness was decreased to 30 nm and to 0.45 eV when the film thickness reached 20 nm. Non-monotonous spectral dependence was observed in 30% of the samples while in imperfect samples it was more difficult to obtain QSE.

There are some typical problems that came around in many papers and with which I became familiar too during the project. A common problem with nanowires is that they tend to be very sensitive to any electrostatic discharges and are easily melted because of the low melting point of bismuth of 272 ˚C. Even if they are handled carefully and being always shortcut except during measurement. This is more problematic if the research is done by sputtering and measuring the same samples several times. It is also very time-consuming if the sample burns after a few measurements. At an early stage of the measurement series there is not enough data points to make any conclusion, but significant amount of time and effort has already been spent to get the measurement series started. Two dimensional film samples are less likely to burn up, but the problem is always that they are formed of several grains with different crystal orientation which may

contribute differently to the overall resistance of the sample. A mitigating fact is that the band structure of bismuth is axially symmetric relative to the trigonal axis, and most crystals seem to be aligned with their trigonal axis along to the substrate surface normal, that is to say, they have a hexagonal form when observed from above. The average grain size should also be larger than the film thickness, otherwise electrons will scatter from crystal boundaries and the QSE will be suppressed [8]. The same author has assumed that lower layers of the films may have different or less perfect crystal structure than top parts. This could partly explain the damping of the oscillation amplitude of electronic properties and changes in its period with very thin films (d < 100 nm), as theoretical calculations always consider a perfect single crystalline structure. Decrease of the oscillation period in decreasing film thickness is important as the metal-to-semiconductor transition is theoretically expected to happen when the film thickness equals the period of the oscillation near the transition thickness. Sometimes a thin metal film quality is better when the evaporation is done on a heated substrate, the optimal temperature is disputed, but is expected to be somewhere between 1/3 T_m and 2/3 T_m, where T_m is the melting temperature of the metal [11].

The author [9] had a different approach for making 1D nanowires. They used porous alumina template with long, straight and smooth hollow channels in it, which were then filled with bismuth. Filling could be done in different ways, either by high pressure injection of molten bismuth, with vapor injection or by electrochemical deposition. Afterwards the alumina template was chemically dissolved free standing bismuth nanowires were obtained, that were then positioned on lithographically manufactured electrodes. According to the author [9], very high quality and very thin (d~7 nm) 1D nanowires were obtained by this method. However, they had serious problems positioning individual nanowires on a substrate for reliable electric contacts. Ultimately they claimed to be able to confirm the theoretically predicted metal-to-semiconductor transition through magnetoresistance measurements [12].

4 Methodology

This chapter discusses the fabrication and measurement processes of the samples step by step. It includes some detailed notifications which are important to know for anyone who might try to repeat or continue the research on single domain bismuth crystals.

4.1 Sample fabrication and preparation

In this work the objective was to produce a single crystal bismuth nanowire connected to two contact pads from both ends so that the resistance could be measured via four probe method. Initial dimension of the nanowire samples were typically 500-700 nm in length, 300-500 nm in width and height, which was limited by the thickness of the resist, was 150-300 nm. General geometry of the samples is presented in Fig. 4.2 at the end of the chapter. Some minor changes were made to contact geometry during the project to achieve a better crystal orientation of the sample.

Samples were made with e-beam lithography on substrates which were circular Cambridge Goodfellow potassium aluminosilicate (muscovite mica) chips that were 0.15 mm thick and 12 mm in diameter. Mica was selected after an intensive literature search as a substrate material whose lattice constant matches with bismuth. Before spinning the resist, the samples were first cleaned in boiling acetone in ultrasonic bath and then by reactive ion etching (RIE) in oxygen plasma. Used resists were commercial PMMA

resists, typically MicroChem MMA (8.5) MAA EL11 for the lower layer and MicroChem 950 PMMA C2 as a copolymer. Lower layer was spun 30 seconds with 6000 rpm and copolymer 30 seconds with 3000 rpm, which gave the total resist thickness of about 500 nm. The exact thickness of the resist was never measured as the recipe worked well, the estimation for thickness was taken from a data table made by our group. Both layers were heated one minute on a hot plate which was at ~160 ˚C temperature. Sometimes I changed the rotation rates, but most of the samples were made by the recipe described above. The only problem which occurred with the resist was that if the copolymer layer was rotated with a too high rate of 6000 rpm, the layer became too thin and could collapse in the vicinity of the sample in where the resist stretched a long way shelf-like without support because of the undercut. If the resist collapsed the formed samples were not usable.

Since mica is highly dielectric the chips also needed a conductive layer in order to be exposed by e-beam. Conducive layer was made by evaporating 10-20 nm layer of aluminum on the top of the copolymer and the chip was then exposed normally with Leo 1430 scanning electron microscope (SEM) with 20 kV acceleration voltage. After exposure aluminum was etched away with 1.4% strong by weight sodium hydroxide (NaOH) solution and the chip was cleaned with deionized water. Aluminum layer had to be removed properly by giving enough time to the sodium hydroxide to etch the layer completely. In some cases a thin transparent film of Al or AlOx was possibly left over, which I suppose caused problems during development. Water cleaning had to be done gently, because a high cohesion of water may have caused resist to be removed from the substrate. Otherwise the aluminum layer and sodium hydroxide and water treatments didn't cause any trouble. Without the conductive layer, the chip got charged during exposure and discharging currents exposed lightning-like patterns in the resist and spoiled the samples. Mica was an ideal substrate because of its dielectricity and also because bismuth formed nice nanostructures on it, making large uniform crystals and a continuous layer. It was crucial that the substrate was a good insulator since bismuth itself is not a good conductor as a metal. Other potential substrates which were tried were silicon oxide and glass, but bismuth didn't form a continuous layer on them. Crystals, even though rather large, were not connected to each other. AFM picture of bismuth film evaporated

on glass is presented in Fig. 4.5, bismuth grains on glass are clearly orientated differently and are very different in sizes.

In order to get large crystals with a characteristic size of about half a micron, the evaporation had to be done in strict conditions and the purest bismuth in our disposal (Goodfellow 99,9999% Bi) was used as evaporation material. Before the evaporation, the chip was once again cleaned with oxygen plasma RIE to remove any residual resist from the developed cavity which could cause defects on the forming crystal. Evaporations were done so that the chip was heated up to 130-140 ˚C, which is as high a temperature as one can go up to without melting the resist all together. Evaporation speed was rather high of about 1 nm per second. Evaporation was done relatively fast, as I tried to minimize the time for any foreign materials in the chamber to condensate on the structure as it was forming and causing defects on the crystal. Evaporation was done in about 10^{-6} mbar vacuum. Unfortunately the vacuum was not the best possible because the whole chamber had to be open before evaporation in order to put the required heating installation in place. Evaporation on a heated substrate is known to be an advantageous method for making large bismuth crystals on a substrate [4]. Heating was done by blowing hot air inside the heating column while the outer side of the column was in the vacuum chamber. The same ´column´ can be used as a cooler for other applications by filling it with liquid nitrogen. The temperature of the substrate was measured from the inside with a thermocouple which was mounted in a metallic bolt in order to increase the heat capacity and to protect the thermocouple from direct flow of hot air, so that the temperature reading would be more stable and hopefully closer to the real surface temperature of the sample. The evaporator was Bal-Tec, Bae 250 coating system. Schematic picture of the evaporation set up is presented in Fig. 4.1.

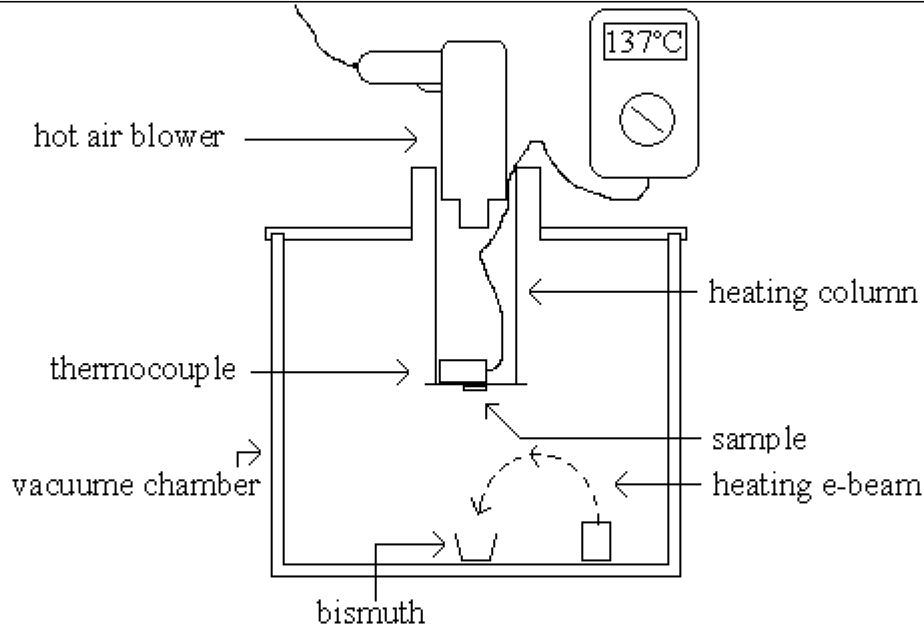

Fig.4.1: *Evaporation setup with the substrate heating installation.*

Newly made samples were observed with Nanoscope IV Digital Instruments atomic force microscope (AFM) in tapping mode and Nanosensors type PPP-NCHR-20 tips. SEM could not be used because of the substrate charging problem. AFM pictures were then analyzed and suitable samples were chosen for measurements. Distinctive hexagonal crystals and their boundaries could be identified in AFM pictures and good samples were those that stretched smoothly from one side of the contact points to another without any grooves or bumps in between. This is of course not as such an absolute guarantee that the sample was formed by a single crystal. During the project I observed a lot of different samples and other bismuth structures on mica, and I recognized that the characteristic size of a crystal was typically around half a micron, which was very close to the size of our structure. Making a genuine single crystal sample turned out to be very difficult and most of the samples seem to be formed of several micro crystals. They were still an interesting subject of study and I could expect to see non-monotonous size dependence of resistance. Another demand for a usable sample was that there had to be at least two good samples on the same chip. Our measuring probe allowed two samples to be measured at a time and measurements were quite time consuming. It took about two hours to measure and sputter a chip if everything went well and as I needed a lot of these

measurement points, it was more sensible to start with two samples on a chip instead of one.

Contacts from the sample holder to samples were made by 50 μm thick golden wires. Gold wires were shouldered to the sample holder and contacts to the sample were made so that the gold wire was positioned on top or close to the bismuth contact pad and a piece of indium was then pressed on top of it, so that it covered the wire and the contact pad. In the beginning I used silver epoxy to make the connection, but it turned out to be problematic and tended to break and got porous during thermal cycling. In addition when it broke and was then repaired, it took one day for silver epoxy to dry up and this would have lengthen the time of measurements to unbearable. I also tried to bond contacts, but mica was too fragile a material for that and broke instantly under the bonder as it used an ultrasonic vibrator to attach the wire onto the substrate. Later I learned that I could re-expose and evaporate the chip and I added larger, about 1×1 mm size copper contact pads to the chosen samples. This helped in making contacts with the indium pressing method and in addition the structure itself would stay intact by this way. This was advantageous as the indium piece used to attach the gold wire to the structure, often removed parts of the bismuth structure too when connection broke and got loose. If that happened often enough, the bismuth contact pad got worn out even if the sample itself would still be usable. Another benefit of making the contacts larger later, was that making four solid square millimetre sized contact pads to each sample by e-beam would have taken a long time and less samples would have fitted on the chip. I also used re-exposure to repair damaged structures. For instance, if a sample's leg was broken only some tens of microns from the sample, this was the only way accurate enough to repair it. Procedures of making a conductive aluminum layer were the same as in the sample fabrication. If the sample had been contaminated with copper or aluminum in the process, the outer layer would still have been removed during sputtering and the inner parts of the sample would stay clean.

During the project, I varied the samples' geometry and dimensions, in order to get a perfect single crystal sample between four contacts. I changed the length and width of the sample slightly, as well as the angle of those parts of the contacts that were near to the sample. All these factors seem to have an effect on the crystal orientation of the sample.

Schematic picture of the samples is presented on the upper part of the Fig. 4.2, under it are the AFM images of three samples with different geometries. In most successful samples the near parts of the contacts had the same crystal orientation as the sample itself, therefore I tried to enforce the crystal in favorable orientation by making 120˚ angle between the contacts and the sample so that the angle would correspond to an angle of a hexagonally shaped bismuth crystal. That procedure was not succesful either, because the corners of the opening of the resist are not sharp and the angles between the sample and the contacts near the sample were slightly larger than planned. I also tried 90˚ angle, but then the crystals orientated themselves in a row, so that their longest diagonals were perpendicular to the sample length, while my attempt was to align one hexagonal crystal with its longest diagonal along the center line of the sample. That has happened with the sample on the lower right side in the Fig. 4.2. A favorable angle seemed to be slightly less than 120˚. Another method, which I thought might help, was to vary the samples size so that it would correspond to a characteristic size of the crystals. The ideal width at half maximum of the sample seem to be about 450 nm. Thinner samples tend to form a row of crystals, while wider could have for example two crystals side by side. If contacts were too wide the crystals in them were usually randomly orientated, and so they didn't support any orientation of the sample what so ever. Most successful samples typically formed when contacts close to the sample were roughly the same width as the sample itself and orientated so that contacts supported the crystal orientation of the sample, as in the picture at the low left in Fig. 4.2. A common problem was that the sample took its crystal orientations from both ends of the wire, which are marked in the schematic upper part of Fig. 4.2 by circles A and B. Those areas had the most available space for the large crystal seeds to start to grow in. In such case the sample was often divided into two separate crystals with the crystal boundary somewhere in the middle of the sample.

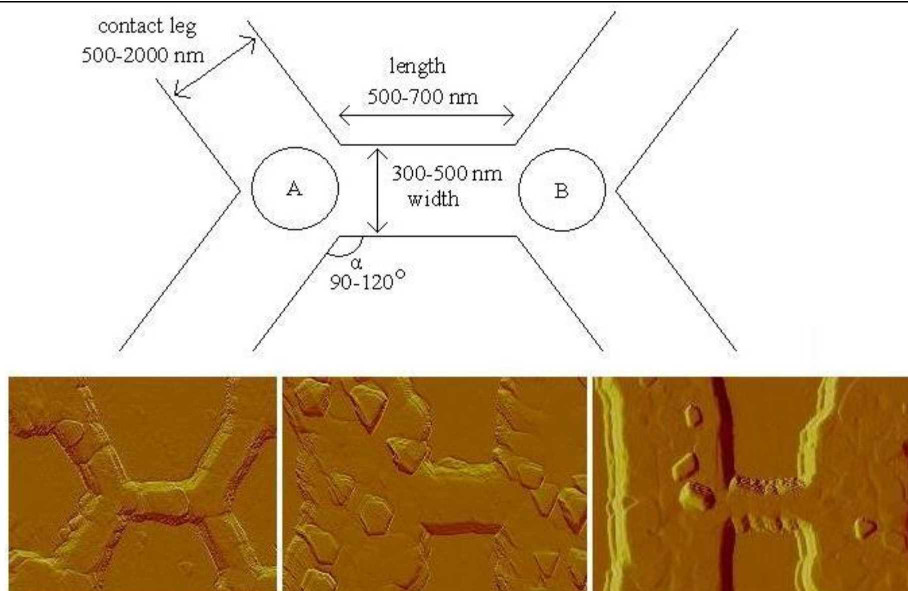

Fig 4.2: *Different geometries of the samples. Crystal seeds often started to grow on areas marked by A and B in the upper part of the picture.*

In Fig. 4.3 there is a three dimensional AFM image of one of our best quasi-single-crystalline samples.

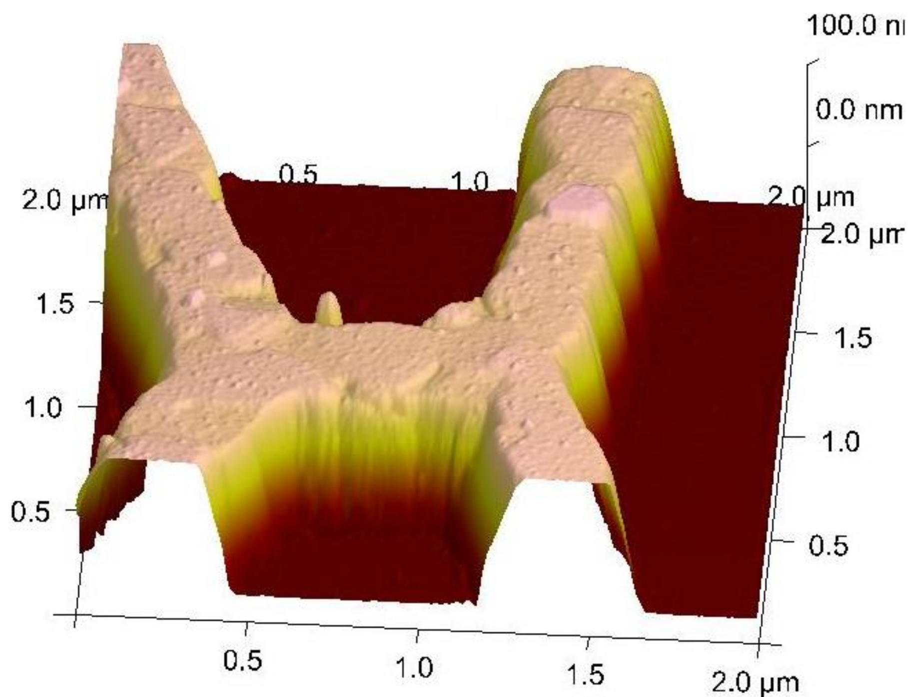

Fig. 4.3: *AFM image of a quasi-single-crystalline Bi nanostructure on mica substrate.*

4.2 Fabrication and structural analysis of film samples

In addition to small nanowire samples, I made two larger film samples. Films were made on the same Goodfellow mica chips as the wire samples, but without e-beam lithography. Instead, they were evaporated through a mechanical mask which was put on direct contact on top of the sample. Samples were 5.0±0.5 mm in length, 0.5±0.1 mm in width, thickness of the first sample was 300±10 nm and the second one was 200±10 nm thick. Lateral dimensions were difficult to measure very accurately at this scale, especially because the contacts were as wide as the sample itself. It was difficult to determine where the contact ends and the sample begins. However, with film samples it was not so crucial to know lateral dimensions accurately, because I was interested in the quantum properties which were related to the film thickness. Average thickness was estimated by a quartz crystal thickness monitor during evaporation. In AFM image in Fig. 4.4 it can be seen, that the thickness varies a lot when some crystals grow much above the average surface level.

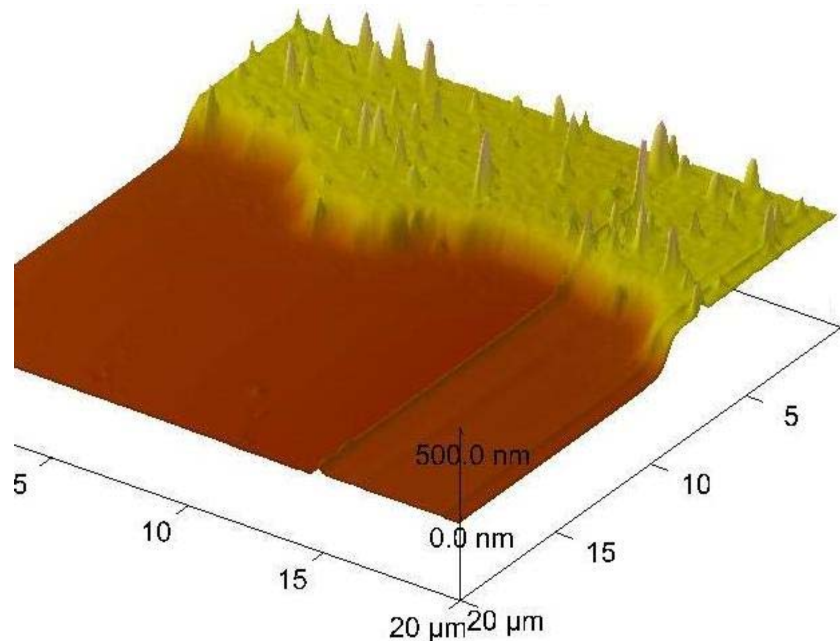

Fig. 4.4: *AFM image of the edge of a 2D bismuth film sample on mica substrate.*

For the comparison of different substrates, in Fig. 4.5 there is an AFM image of a bismuth film grown on glass, quality is clearly not as good as in the film evaporated on mica.

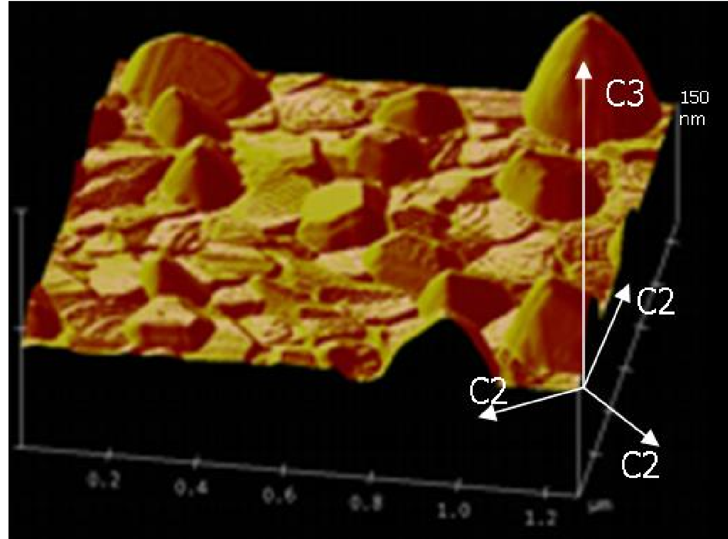

Fig. 4.5: *AFM image of a bismuth film on glass. Individual crystals can clearly be identified.*

4.3 Measuring setup

Measurements were made by the four probe method using AC and DC currents in a range between 10 nA and 1 μA. Measuring frequency in AC measurements was19 Hz. Sometimes I checked the sample by using different frequencies, but the resistance was always calculated from the measurement values taken at 19 Hz AC. For wire samples the measurements were typically made with 10 nA current and for film samples with 100 nA. DC mode was mainly used to confirm the result and I held the previous AC result as a reference when observing the changes in resistance. Various batteries, electronic current sources and voltmeters were used in different DC measurements, since some of the equipment were not always available, but AC set up was the same in all measurements. AC and DC measurement set ups didn't share any common parts except one 1 MΩ resistor, some coaxial cables and the dip stick itself with filter components to reduce

environmental EM noise. Block diagrams of the AC measurement set up and dipstick filtering are presented below in Fig. 4.6. Measurements were made in four probe configuration so that current went through the contacts with the same letter, for example from A^+ to A^- in the picture, and voltage was measured from other two contacts with the same letter. In Fig. 4.6 the voltage probes are marked with B^+ and B^-. Contacts with the same letters had filtering between them which is drawn on the right side of the picture. Signal was taken from Stanford research system Model DS 360 signal generator, the voltage over the sample was amplified with NF Electronic Instruments LI-75A low noise preamplifier with gain of one hundred. Measurement value for voltage was read from NF Electronic Instruments LI-575 lock-in amplifier and the phase and shape of the original signal and the measured one were compared with Tektronix TDS 2014 oscilloscope. Current was checked before the measurement with Stanford research system model SR 810 DSP lock-in amplifier. Contact to current monitor was grounded during the measurement as the current monitor seemed to cause some small disturbances to the signal. All the devices got their power from Furman AC line voltage regulator Model AR-2330 except preamplifier which was powered by a 12 V battery.

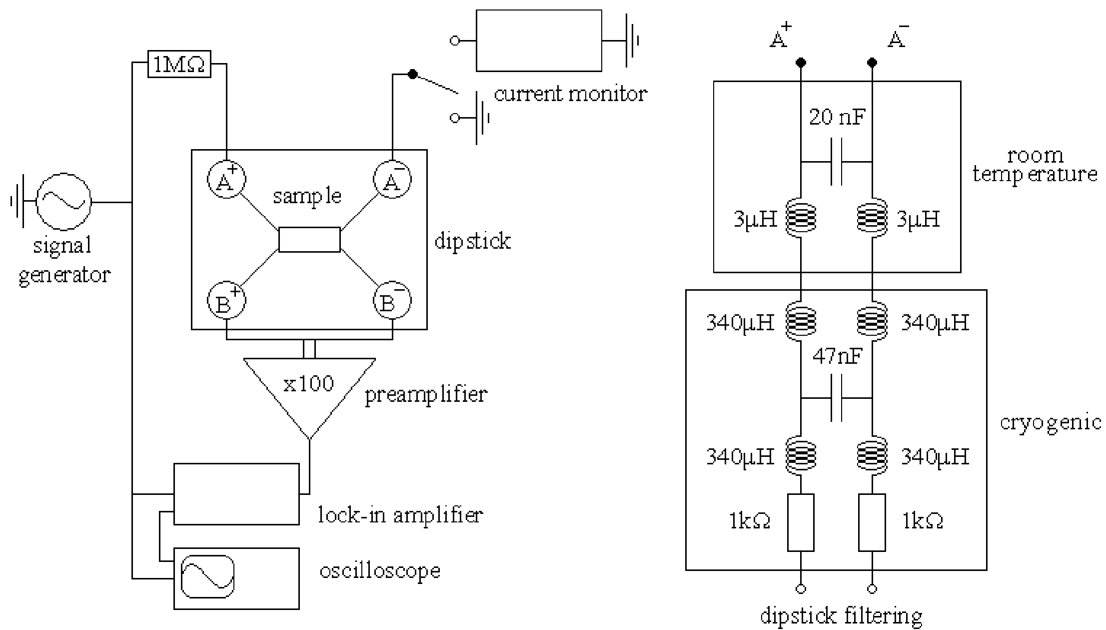

Fig. 4.6: *On the left the AC measurement set up, on the right the filtering configuration of the dipstick.*

Cooling downs from room temperature to 77 K were done in a time span of about five minutes and from 77 K to 4.2 K in about 15 minutes. Heat ups were done in dry nitrogen flow so that moisture would not condense on the samples and cause any possible damage. That took about twenty minutes. Samples were stored in a vacuum box to protect them from moisture and oxidation in atmosphere. Between measurements the samples were reduced in size by ion beam sputtering.

4.4 Sputtering setup

Sputtering was done with tectra GmBh Physikalische Instrumente ion gun, using argon ions, typically with 0.6 kV acceleration voltage and 45˚ incident angle. In this thesis the mentioned sputtering angle always means the angle between the beam and the chip's surface, not the angle between the beam and the surface normal. Both definitions are used in different papers about sputtering. Later I started to sputter samples only from the sides, so that the sample's axis was always perpendicular to the beam and the sample was turned 180˚ repeatedly. By this way the sample was consumed more from the sides and therefore maintained a better aspect ratio, additional benefit was that the contacts were consumed less relative to the sample. During single sputtering sessions the consumption of the surface of the samples ranged from a few atomic layers to tens of nanometers. Beam current was measured with a brass mesh which was positioned about 0.5 cm above the sample. The mesh was to gather the charge carried by the beam, so that it would not only be used to measure the current, but also to neutralize the beam before it hit the mica chip and the sample. Sample was manually rotated and it was shortcut but not grounded, so it may be that the chip got charged during the sputtering. The mesh's cords were 100 μm thick which formed 400 μm wide squared openings. The neutralization ratio of the ions has not been precisely defined for not being quantitatively important. Pressure in the chamber was optimized every time for the fastest possible sputtering rate and was $(1-4)\times 10^{-4}$ mbar. Semantic picture of the sputtering installation is represented in Fig.

4.7. Sputtering is discussed with more detail in the next chapter, as it has some technological interest of its own.

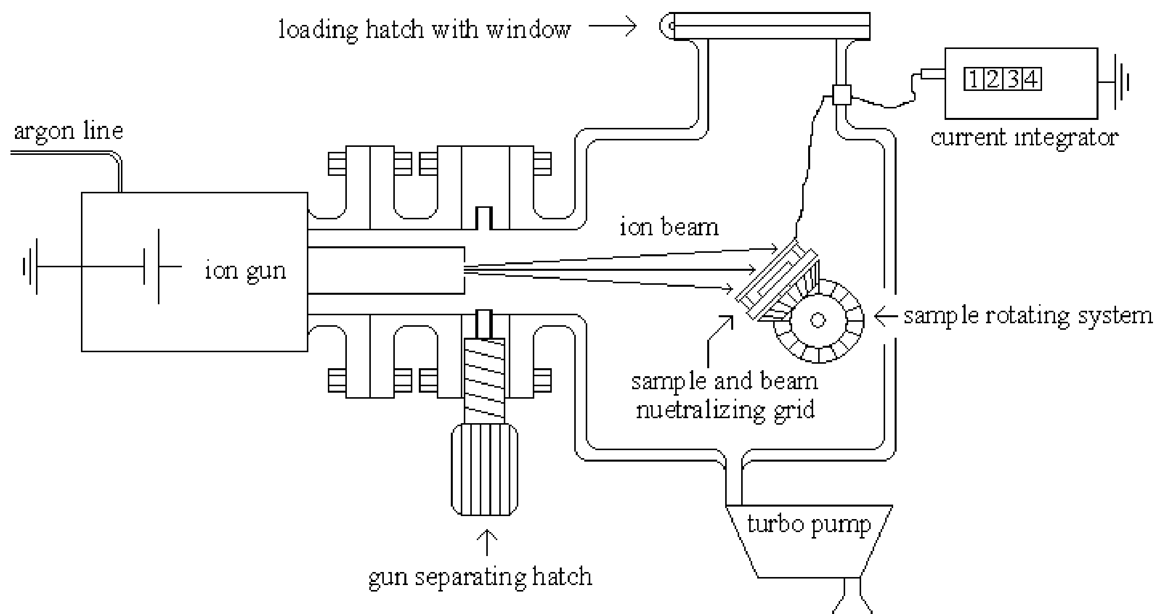

Fig. 4.7: *The sputtering set up.*

5 Results and discussion

Results chapter is divided into sub chapters, the first discusses the sputtering related issues and the later one concentrates on the QSE, the main subject of the thesis.

5.1 Sputtering

Sputtering of samples with ion beam was used just as a tool in this research, but I want to put weight on the discussion of the process because it is not that widely used method in nanotechnology research and because it can be applied in completely other fields of research and industry too. It was also one of the important subjects and motivation for this thesis.

Lithographical methods have a limited resolution in patterning. Fundamental limitation is set by the wavelength of the radiation that is used for the exposure. If one wants to make measurements with smaller samples, the sputtering of originally larger sample is an alternative method to fabricate them. An additional benefit of sputtering method, particularly when size dependent effects are studied, is that one and the same sample can be used for measuring the properties of different size structures. This assures that the measured changes in properties are at least much more likely to be caused by the changes in size, and are not some unique peculiar property of an individual sample. It must be noted that this method can not be used to increase the packing density of any

components however, as it depends on the original manufacturing method. It can only be used to downsize the sample, which has been made by other means. Reducing the dimensions of nanostructures by ion beam sputtering was developed and successfully used in our group, and at first the method was applied to reduce the size of aluminum nanowires and single electron transistors [13, 14, 15 and 16]. Later it was applied to bismuth nanowires in a study [3] where some non-monotonous behavior of resistance relative to the cross section of the wire was observed.

By ion beam sputtering the consumption of the surface can be adjusted with the accuracy of a few nanometers, which is generally much better than by wet etching methods without using any stopping layers. Accuracy obviously depends on the overall amount which is sputtered during a single session, but with careful adjustment, in the case of bismuth, it was possible to remove practically single atomic layers during a sputtering session. Ion beam treatment is also likely to polish the surface and make the samples more homogeneous if the incident angle of the beam is varied during sputtering. Studies made with aluminum nanowires show that if the angle of incidence is not changed the surface roughness may even increase as the different grains have different crystal orientation and are therefore consumed with different rates when sputtered from the same direction constantly [18].

Consumption of the bismuth was measured with test film with initial dimensions of 5 mm in length, 0.5 mm in width and 300 nm thick. Initial resistance of the sample was measured to be 61.1 Ω. Literature value for that size bismuth sample would be 43 Ω, if resistivity is assumed to be the same as for bulk. Changes in thickness inflicted by sputtering were measured by comparing the room temperature resistance of the sputtered film to the initial value. It was assumed that the QSE will not show significantly at room temperature and in the thickness range of 200-300 nm and that the relative consumption of lateral dimensions is negligible, so that the resistance would therefore be proportional to $1/d$, where d is the film thickness.

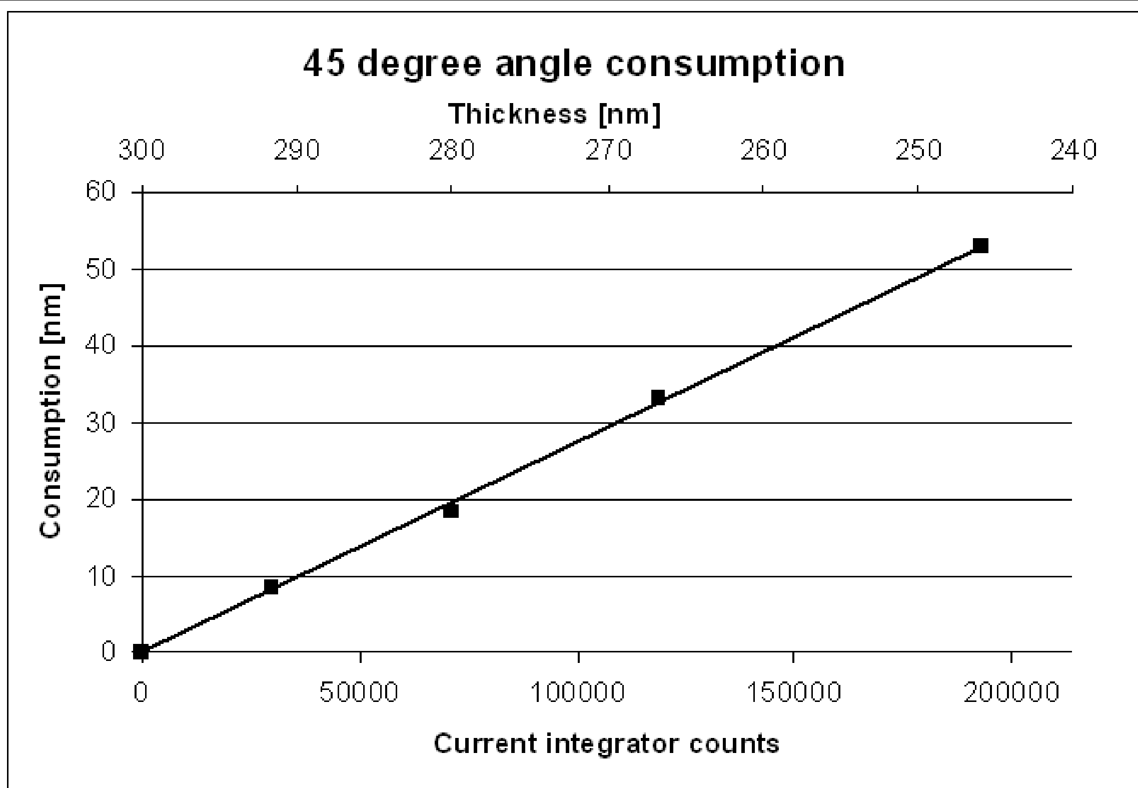

Fig. 4.8: *When sputtered with Ar^+ from 45˚ angle with 0.6 kV acceleration voltage the Bi consumption rate was (0.27±0.01) nm/1000 counts. Initial thickness of the sample is measured with AFM and was 300±10 nm, evolution of the thickness is estimated from the changes in the room temperature resistance of the film. Final thickness is estimated to be 250±10 nm.*

In the first series of measurements the bismuth film was consumed by 53 nm in four sessions in which incident angle was 45˚ and acceleration voltage of ions was 0.6 kV and the sample was rotated randomly during the sputtering. After the measurement series the resistance of the sample was 76.4 Ω. Least mean square fitting of the consumption is presented in Fig. 4.8. Equation of the line is (0.274±0.003) nm/1000 counts. So the film was consumed by 0.272 nm (which is of the order of lattice constant in bismuth) for every one thousand counts of current integrator counts. Most of the error in the consumption rate came from the error of determining the initial thickness of the film, which was ~3%, the error of mean least square fitting was only ~1%. Sputtering a thousand counts typically took several minutes, this means that one could easily adjust

the total consumption of the sample with the accuracy of few nanometers, depending on the total length of the session. It may be that there was a thin natural oxide on the surface and that consumption rate would therefore have been different when very short sputterings were made. In some cases it seemed as if during very short sputtering sessions the consumption rate of the surface was less than during longer ones, which can possibly be explained by the oxide layer. Otherwise the accuracy overexceeded my expectations. After the first sputtering experiment I continued with the same sample and consumed it 40 nm more but now from 90˚ incident angle. Consumption rate was then higher (0.441±0.006) nm/1000 counts. After the measurement series the resistance of the sample had increased to 87.8 Ω. Linear least mean square fitting of the later measurement of consumption versus the amount of used ions is presented below in Fig. 4.9. From these consumption rates, the consumption in the direction of the beam can be calculated by dividing the first one by sin α, where α is the incident angle of the ion beam. Consumption rate in the direction of the beam was 0.38 nm/1000 counts for 45˚ angle and obviously the earlier mentioned 0.44 nm/1000 counts for 90˚ angle. Consumption rates in the beam direction do not differ very much. Highest consumption rate (sputtered atoms / used ions) is not achieved by 90˚ sputtering angle but with some intermediate angle between 0˚-90˚. This can be understood so that when the angle starts to increase from 0˚, the energy that ions introduce to the surface is increasing, but also a reflection rate of ions changes as the angle changes. In Ref. [19] InP was sputtered with acceleration voltages between 500-1500 keV and it was found that the optimal angle depends somewhat on the acceleration voltage, but is always different from 90˚. The beam intensity and the number of ions hitting the surface are obviously always at their highest with the 90˚ sputtering angle.

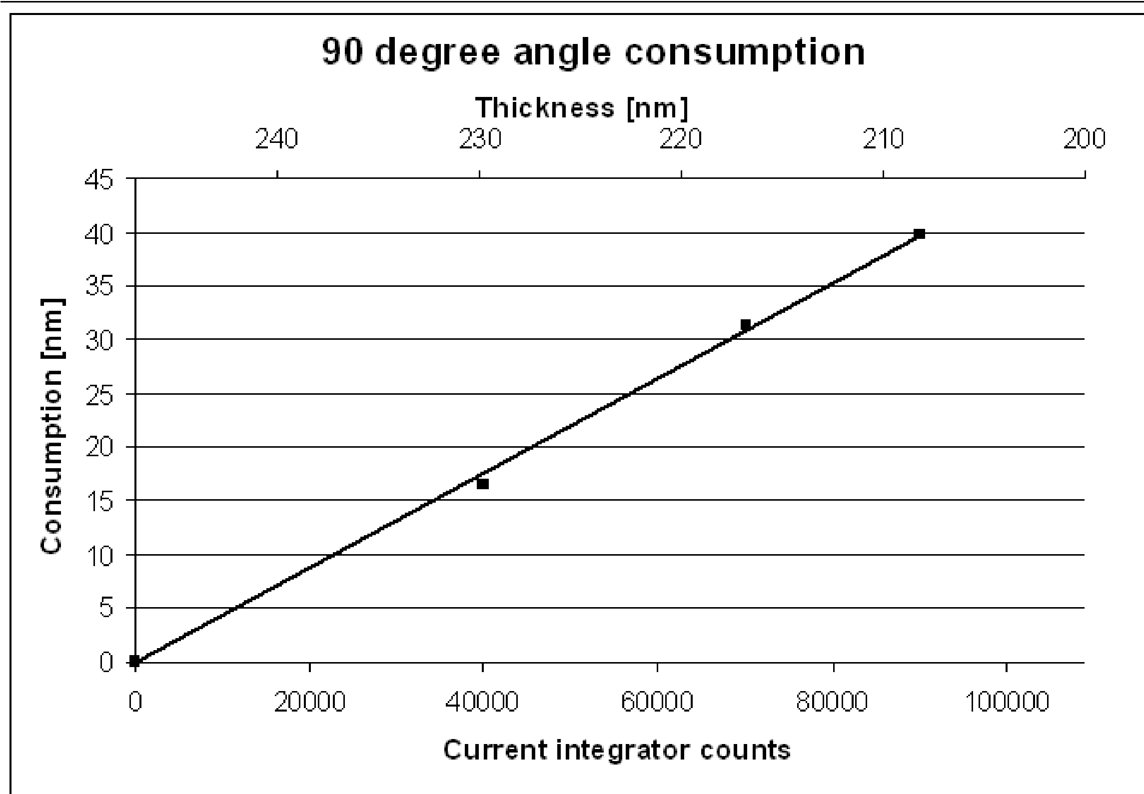

Fig 4.9: *For 90˚ angle and 0.6 kV acceleration voltage the consumption rate was (0.44±0.02) nm/1000 counts. Initial thickness was 250±10 nm and final 210±10 nm.*

Consumption experiment showed that in principle the ion sputtering method can be extremely accurate. Unfortunately the joy turned out to be short lived. The sputtering chamber happened to be used as a loading chamber for one of our evaporators and as it was in intense use the chamber was probably chemically contaminated by pump oil or some other impurities, which probably affected the sputtering rate during later sessions. The sputtering rate was also affected some times when the ion gun was previously used for different purposes and by different ways, and most likely every time when the whole system was overhauled. Other problem was probably that during long sputtering sessions the substrate might get charged and consume with different rates in different areas if sample was not rotated constantly. During long sputterings I rotated the sample every five minutes which probably was not frequent enough. After all it is difficult to say for sure, what caused all the differences in sputtering but successful tests proved the validity and

accuracy of the method in principle, if it is taken good care that the sputtering conditions do not change.

In Fig. 4.10 there is a collection of pictures of one of the film samples. On the top (a) there is an AFM image and the cross section profile of the edge of the newly made sample which is 300 nm thick in average. In the middle (b) AFM image and the cross section profile of the sample at the end, after when it has been used for both the previously mentioned consumption tests and for other measurements. Pictures are not from the same part of the chip as those taken from the brand new sample, because it was impossible to find the very same spot from the large sample with the accuracy of a micrometer. In the undermost (c) there are a few optical pictures of the totally consumed sample. It can be seen from the optical microscope image that the sample is not consumed homogeneously, so the resistance is obviously no longer a good measure for the sample thickness. In (b) section a small double step can be seen in the edge profile and in the 3D picture. It is most likely the interface between the mica substrate and the bismuth film and caused by different consumption rates of the materials. Rough estimation can be made from the profile that the bismuth film on top of the mica pedestal is 30-50 nm thick on average, and has been consumed about 260 nm and the mica substrate has consumed about 110-130 nm. On top of the film there is a cone nearly 200 nm high and about as high as the cones in the newly made sample, indicating that the absolute size of the initial roughness has not really decreased in this case.

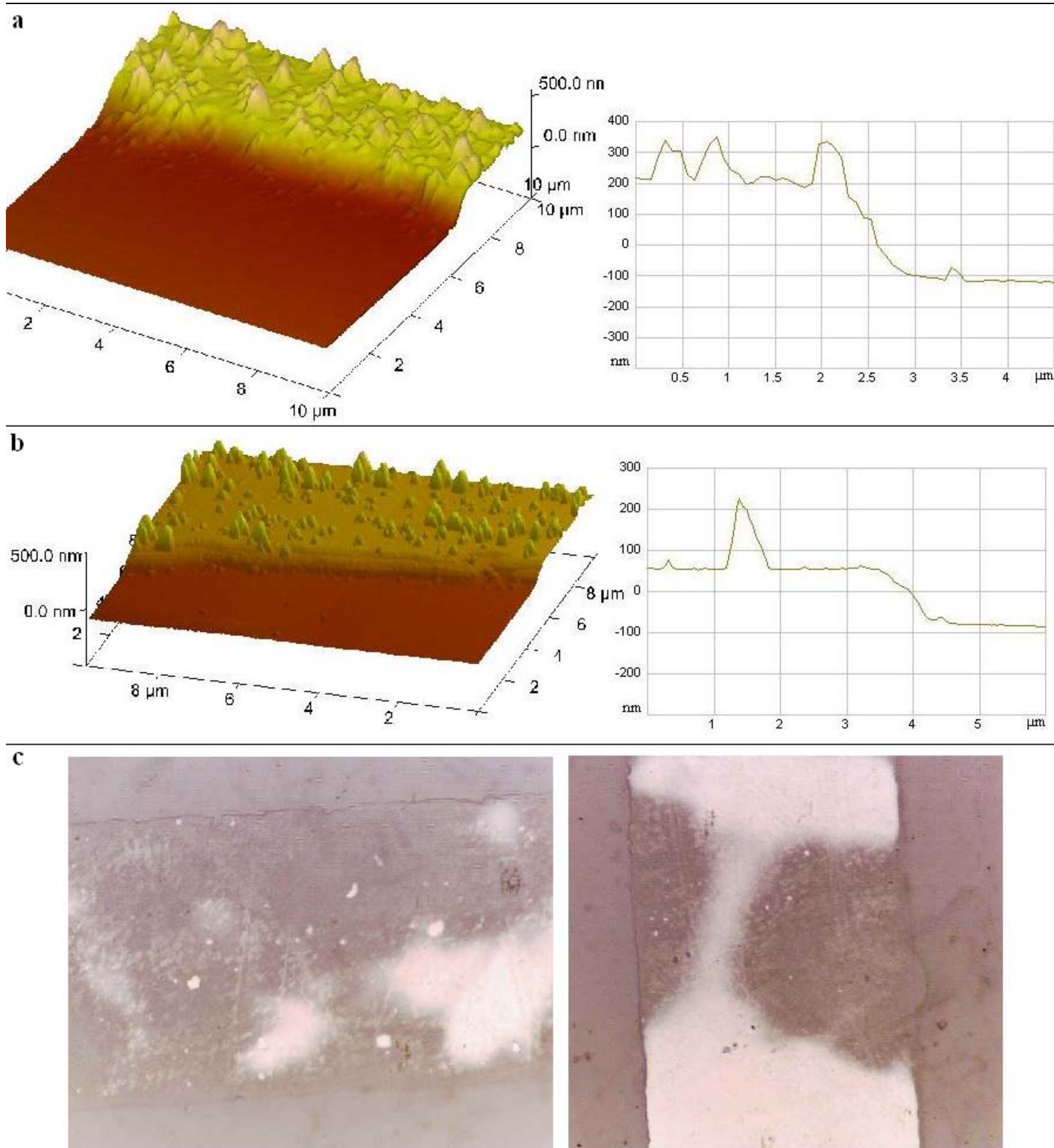

Fig 4.10: *(a) AFM image and profile of the edge of a newly made sample. (b) AFM image and the profile of the sample after several sputtering sessions. (c) Optical images of the sputtered sample. This sample was sputtered in various ways and with acceleration voltages ranging from 0.6–1 kV in different experiments related to sputtering.*

In Fig. 4.11 there are pictures of samples before and after sputtering. This chip was sputtered only from the sides with 0.6 kV acceleration voltage and was rotated 180˚ repeatedly. Upper pictures represent the brand new samples, and bottom images are the same samples after been sputtered 102 000 counts. Two right side pictures of the new samples have some bumping lines caused by some disturbances which are not part of the real structure, but are probably coming from the AFM measuring software. All the samples are from the same chip and they are all viewed from the same direction relative to the chip in all pictures. Pictures of the sputtered samples look as if the same crystal order stretches on all over the scanned area and that the crystal orientation of all the samples is similar because of the similar geometry of the structures. Here again the initial cones that can be seen in the new samples have not decreased, but increased in size, all though their sharp tops have flattened. Cones also seem to have similar triangular form and all of them have the same orientation.

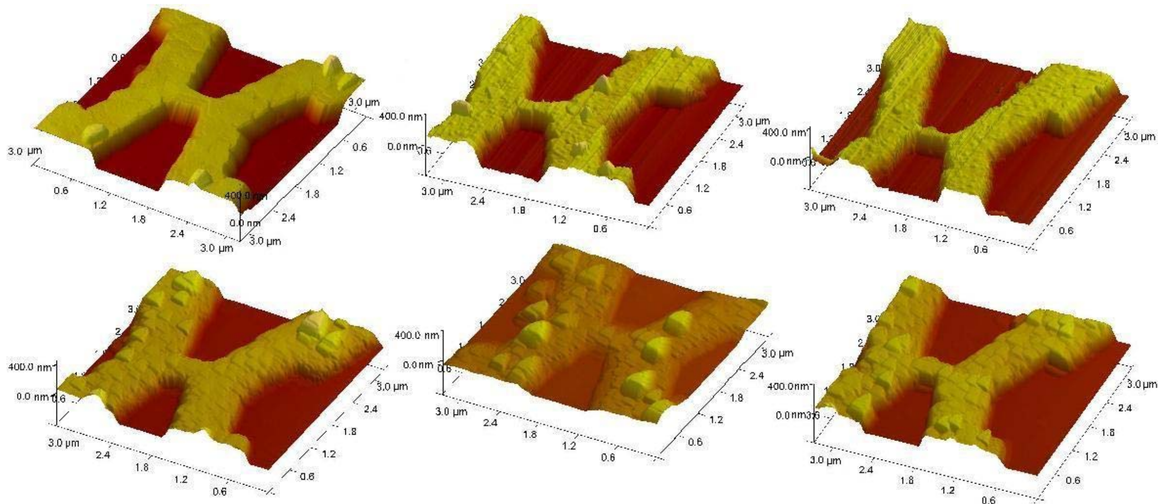

Fig. 4.11: *Wire samples from a chip which have been rotated 180˚ repedeatly during sputtering. On the top the samples in the beginning, in the bottom pictures of the same samples after being sputtered 102 000 counts with 0.6 kV acceleration voltage.*

In Fig. 4.12 there are AFM pictures and cross section profiles of a sample which was sputtered only from the sides of the wire and with 45˚ incident angle but now with 1

kV acceleration voltage. On the left the newly made sample, on the right the sample after been sputtered 40 000 counts.

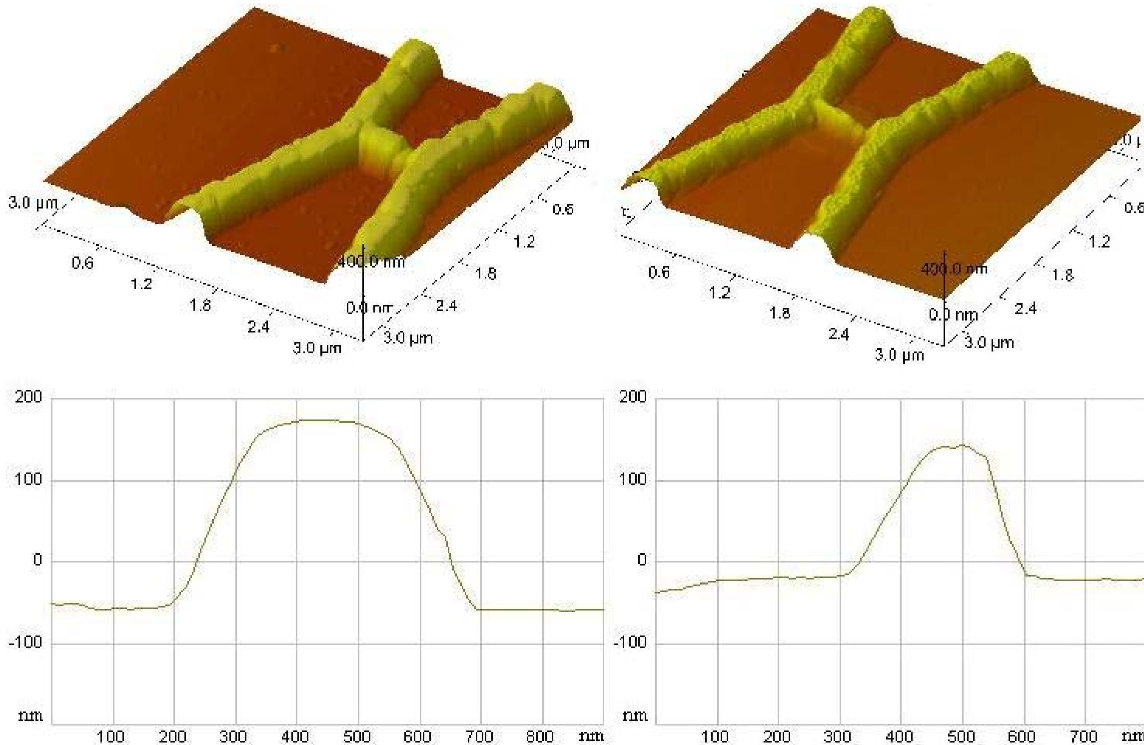

Fig. 4.12: *A bismuth sample and the cross section profile of its middle part before and after sputtering. This sample has been sputtered perpendicular to the wire. New sample is on the left and the sputtered one on the right. This sample has been sputtered 40 000 counts with 1 kV acceleration voltage from 45° angle to the plane and always perpendicular to the wire samples center line.*

Cones of the sputtered samples that appear in the in figures 4.10 and 4.11 could have several explanations. It could be that the crystal structure of the top part may have been less perfect than in the lower layers due to some disturbance during the evaporation process which would have interfered the crystal formation, and then during sputtering the less perfect part could have been removed more easily. In study [20] zinc was sputtered and was found to form different regular textures on the surface due to the anisotropic hardness of the nanocrystals. Changes in chemistry of the chamber may also cause differences in sputtering rates and different crystal faces may have different chemical

properties. Even the intensity of the beam can influence the formation of the cones in single crystal structures. Different surface deposition densities, surface binding energies and incident angle of certain crystal faces to the beam may result in different exotic patterns in sputtering result [21]. Crystal lattice also forms channels in between atomic layers which open in some particular directions and allow ions from those directions to penetrate deeper in to the structure without causing any significant effect on the surface, implying that the consumption would be less with certain incident angles. Bismuth forms hexagonal crystal structure on top of the mica surface resulting from the cubic cell of bismuth, as can be seen in Fig. 2.4. This leaves open channels in three different directions in up angles from where ions may go deeper, there might be other direction as well which offer narrower but wide enough channels for argon ions to go down into the structure. This effect should however be homogeneous all over the structure with the same continuous crystal orientation and cannot explain why cones would form on some particular places.

By using SRIM [23] freeware simulation program[1], I calculated, that 1 kV argon ions should penetrate to about 2-3 nm deep in to the bismuth structure. This implies that sputtering method utilized in this work can be considered as virtually non-invasive. Simulation did not take the contribution of the channels in the crystal lattice to the penetration depth into account.

5.2 QSE Measurements

The main interest of this thesis was to observe QSE in thin films and nanowires. Due to practical reasons the absolute cross section of the wires and films was difficult to determine between measurements, the resistances are presented as a function of beam current integrator counts. Changes in sputtering parameters and conditions mean that

[1] SRIM (the Stopping and Range of Ions in Matter) simulation is a useful freeware program in which input parameters are the ion with acceleration voltage and the target material. The program returns the stopping power per unit length and the average penetration depth of the ions. Program can be downloaded from www.srim.org.

'counts' are not comparable between different samples and in some cases not even between different measurement points of the same sample. Some estimation of the evolution of the sample can be made from the room temperature resistance, which increases homogeneously in most cases and should not be affected significantly by QSE. Estimation of the thickness or cross section of a sample is made by using the initial, very accurately measured cross section, and from the difference of the initial and the final room temperature resistances. Assuming that the room temperature resistance is proportional to $1/d$ and that cross section d decreases linearly over the beam current integrator counts, so the cross section and thickness values are indicative.

In the next chapters the 3D AFM images and cross section profiles are presented and graphs are plotted with three different resistance values corresponding to resistances in three different temperatures 295 K, 77 K and 4.2 K. Measurement points are shown in the inset of the graph, to make the main plots visually easier to follow. Plots are not fitted to data points but are set to go through them. Oscillation of resistances can be seen only in the regions where measurement points are densely packed, in between the resistance increases more or less smoothly and homogeneously because of the lack of data points. Obviously one could expect oscillatory behavior of resistances in these regions as well, if the measurements had been made. Longer sputtering steps were necessary as the samples survived only a limited number of measurement cycles. Samples were measured as long as they survived and the measurement series with wires always ended when the samples were burned, so there are no images of samples after the measurement series.

From my own experiences during the work I would state, that an ideal setup for measuring QSE by using ion beam sputtering to reduce the size of the sample, would include an ion gun and measurement contacts in one cryogenic chamber, which would be at liquid helium temperature all the time. One measurement and sputtering round could then be made in a matter of minutes instead of hours and such configuration would also significantly reduce the risk of destroying the sample by static discharges, as it would not have to be moved around. By this way a sample could possibly be measured to the end in a single day instead in a month. Another benefit may be that the sputtering conditions would stay more stable during the measurement and the reducing of cross section would

therefore be easier to adjust. On the other hand, sputtering in cryogenic temperatures can be somewhat different than sputtering in room temperature.

5.2.1 QSE measurements of the film samples

Film sample 1 was the same sample that was used for sputtering consumption test in Fig. 4.10. QSE measurement series started after the consumption tests had been finished and the room temperature resistance of the sample was then 88.7 Ω. Initial thickness at the beginning of QSE measurements is estimated to be 210±10 nm. At the end the resistance was still a reasonable 187 Ω, but the sample was so unequally consumed, that the measurement series was decided to be closed. Sample was sputtered from 45˚ angle with 0.6 kV acceleration voltage and was rotated randomly. Evolution of resistance of the sample versus ion beam current integrator counts is represented in Fig. 4.13.

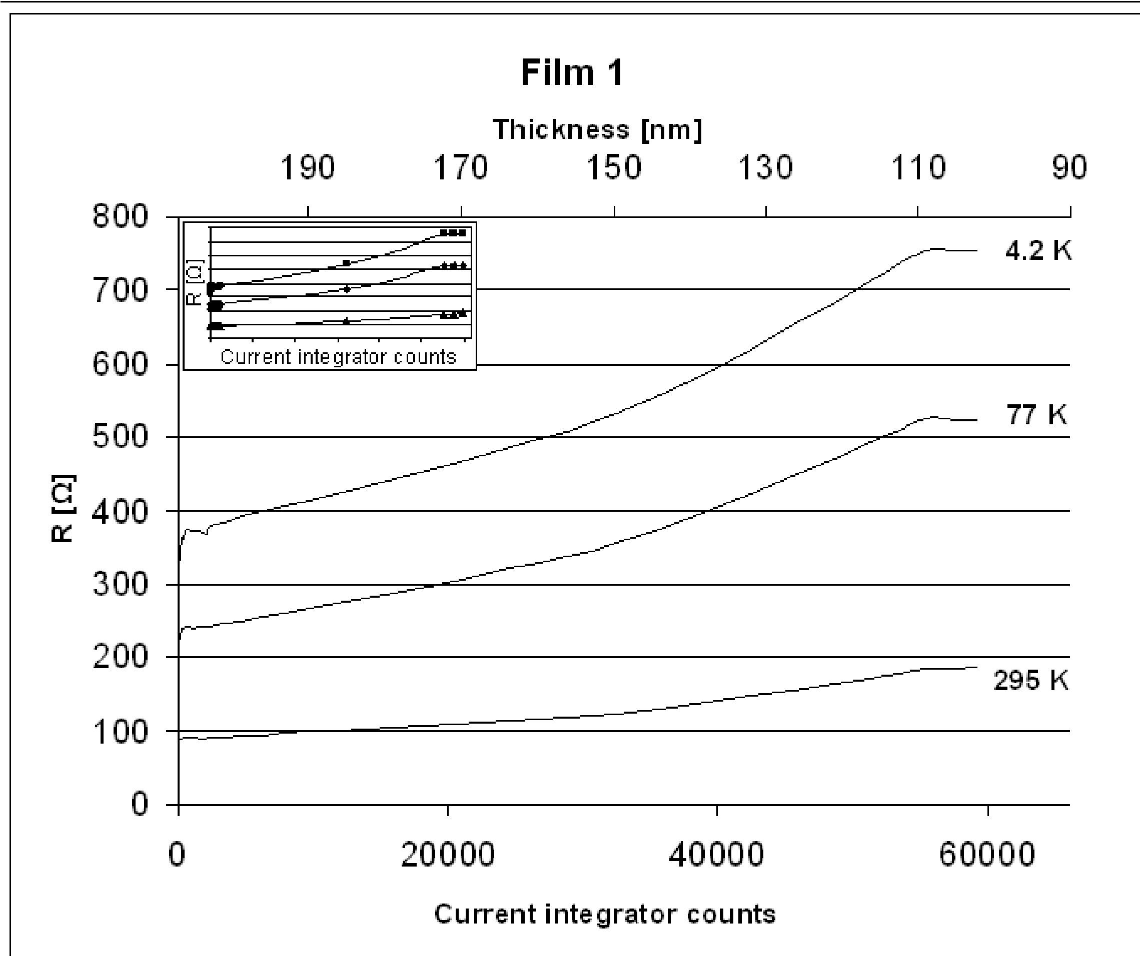

Fig. 4.13: *Evolution of the resistance of the film sample 1 after been first used for sputtering consumption tests. Initial average thickness before QSE measurements of the sample was 210±10 nm and room temperature resistance 92 Ω. The sample was sputtered 60 000 counts from 45˚ angle with 0.6 kV acceleration voltage and it was rotated randomly during sputtering. Final room temperature resistance was 187 Ω, final thickness is difficult to estimate since the film was not consumed homogeneously. Inset shows the measurement points of the plots.*

Initially the average thickness of film sample 2 was measured to be 200±10 nm by the crystal thickness monitor during evaporation and was confirmed by AFM analysis. However, some crystal cones seem to protrude much above the average surface level. Length of the sample was 5 mm and width 0.5 mm, lateral dimensions were the same as for the first film sample. Initial resistance of the film in room temperature was 89 Ω.

Theoretical value for resistance for a sample of this size and using bulk parameters would be 65 Ω. Sample was sputtered with 0.6 kV acceleration voltage from 45˚ angle and was rotated randomly. Measurement series ended after the sample was sputtered 134 500 counts, when some parts of the sample seem to be already completely consumed away and as the resistance curves seem to rise rather fast. Initial AFM picture and cross section profile of the edge of film sample 2 are presented in Fig. 4.14. The evolution of resistance over the sputterings is presented in Fig. 4.15.

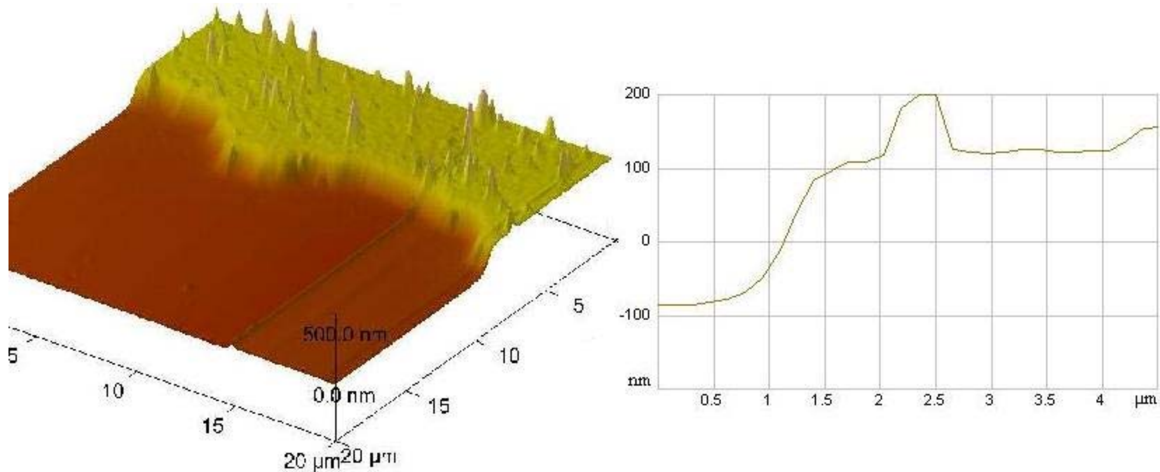

Fig. 4.14: *3D AFM image and the cross section profile of the film sample 2 at the beginning.*

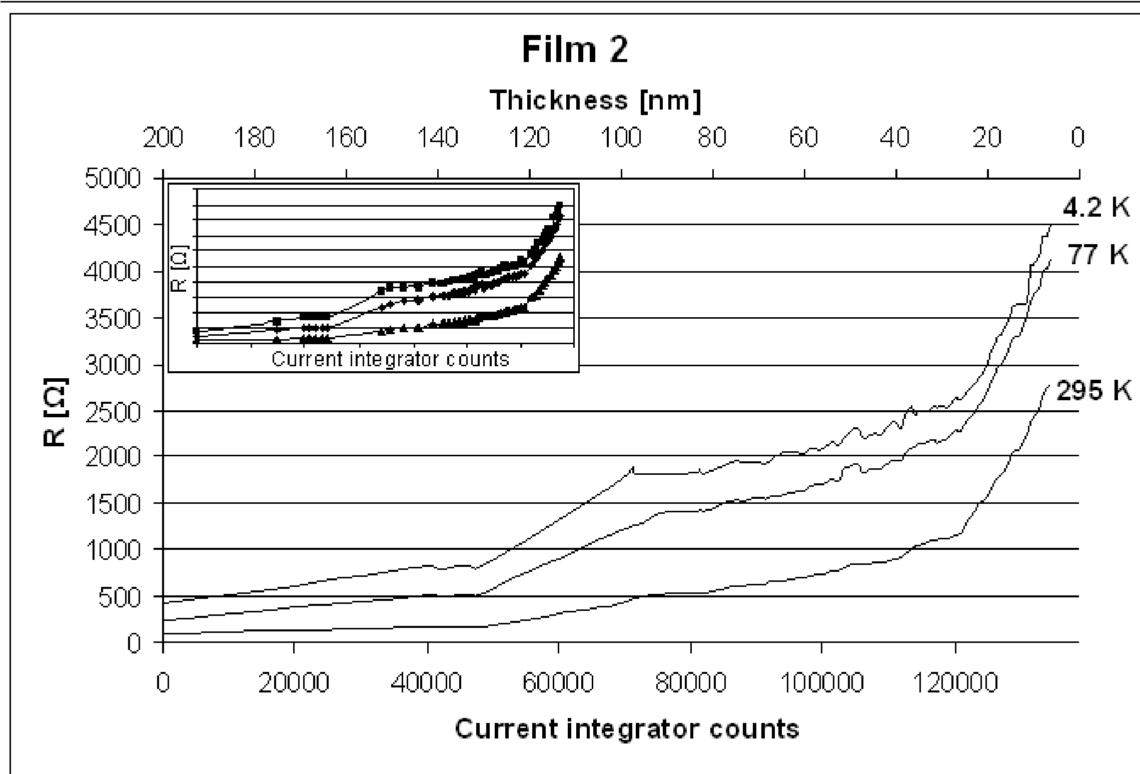

Fig. 4.15: *Evolution of the resistance the film sample 2. Initial thickness was 200±10 nm and room temperature resistance was 89Ω. Sample was sputtered from 45° angle with 0.6 kV acceleration voltage. Sample was sputtered 134 500 counts after which the room temperature resistance had risen to 2780 Ω. Inset shows the measurement data points.*

5.2.2 QSE measurements of the wire samples

Dimensions of all the wire samples are presented in Table 1. Table also shows initial and final room temperature resistances of the samples and the total amount of the beam current integrator counts of sputtering. Change in room temperature resistance can be used to estimate the change in the cross section of a sample. As can be seen in Table 1, coincidentally the final room temperature resistance of two of the samples was 109 Ω and other two happened to have the final resistance of 150 Ω.

Table 1: *Dimensions, total sputtering counts and initial and final room temperature resistances of the wire samples.*

Wire sample	Width [nm]	Thickness [nm]	Length [nm]	Initial resistance at 295 K [Ω]	Sputtering counts	Final resistance at 295 [Ω]
1	490	157	490	21	120 000	150
2	365	172	790	66	195 000	109
3	300	170	660	104	75 100	150
4	325	195	505	41	39 500	109

Wire sample 1 was the first nanowire sample which was suitable for the measurement, as it seemed to have relatively good crystal structure and it survived five measurement cycles. It was also the first ‘practice’ sample, so the measurement series is not the best possible. The first round helium temperature resistance has not been measured and the sample was probably sputtered away with too large sputtering steps in the later stages. On the other hand, as the measurement series was done relatively fast in, one week, and as the ion gun was not in very intense use at that time, the sputtering conditions have probably stayed very stable. In theory and according to previous studies, some oscillation of resistance should still have been visible even with these relatively sparsely located measurement points This measurement series gave some hint about how fast bismuth nanowires are consumed. Sample was sputtered with 0.6 kV acceleration voltage from 45˚ angle and sample stage was rotated randomly during sputtering. Initial room temperature resistance on the sample was 20 Ω. The measured series ended when all contacts showed infinite resistance. In this sample the crystal structure is visible especially well. 3D AFM image and the cross section profile of wire sample 3 are presented in Fig. 4.16 and the evolution of the resistances in Fig. 4.17.

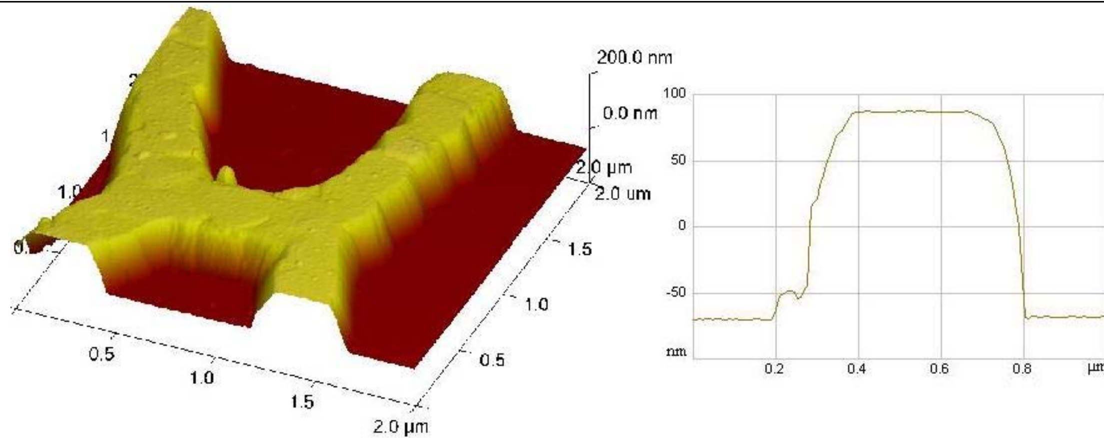

Fig. 4.16: *A 3D AFM image and the cross section profile of wire sample 1 initially.*

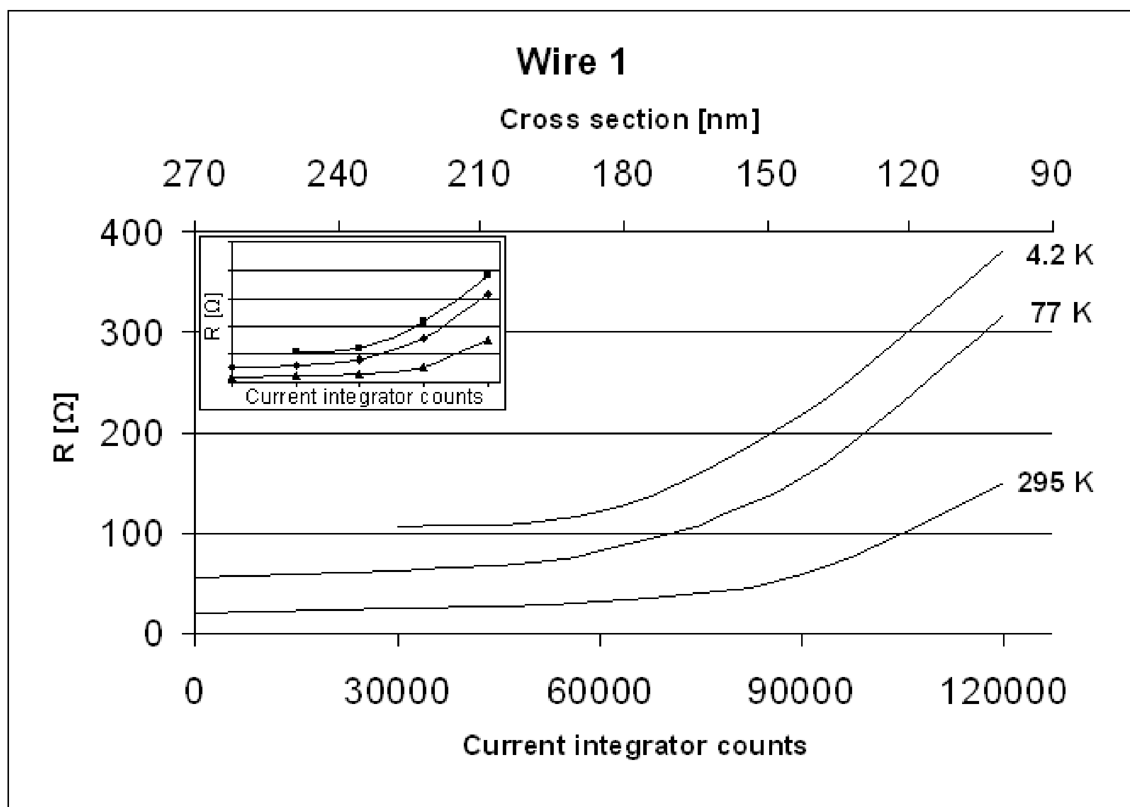

Fig. 4.17: *Evolution of the resistance of wire sample 1.The sample was sputtered 120 000 counts from 45˚ angle with 0.6 kV acceleration voltage. Initial room temperature resistance was 21 Ω and the last measured room temperature resistance was 150 Ω. Inset shows the measurement data points.*

Wire sample 2 was sputtered with 0.6 kV acceleration voltage from 45˚ angle and it was rotated randomly during the process. Initial resistance of the sample was 66 Ω. Room temperature resistance dropped to 58 Ω after the first sputtering. This drop could possibly be related to QSE or more likely, it is due to surface polishing effect since the initial roughness of the sample is considerable compared to its overall size. Sample broke during the last cool down to 4.2 K, after been sputtered 195 000 counts total. Room temperature resistance was then 109 Ω. AFM image and cross section profile of the sample are presented in Fig. 4.18 and evolution of the resistance in Fig. 4.19.

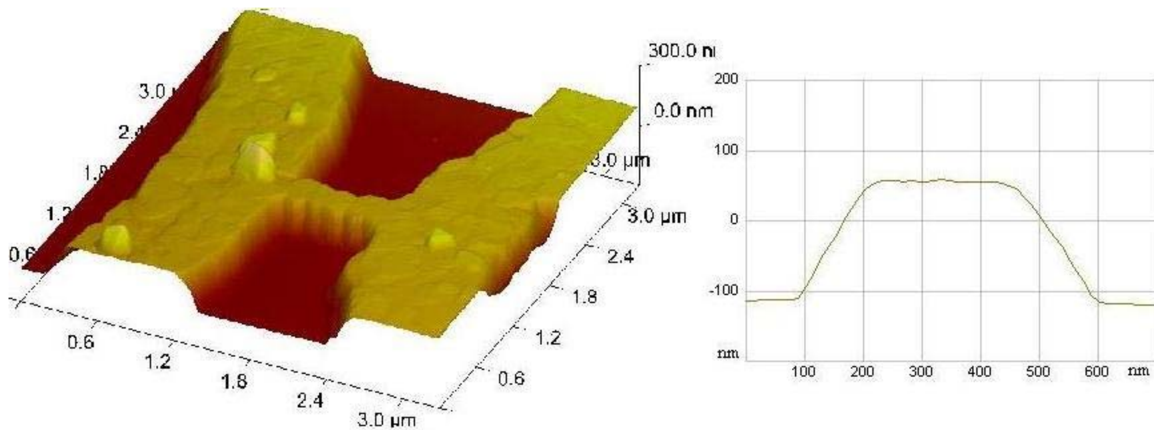

Fig. 4.18: *3D image and the cross section profile of wire sample 2 initially.*

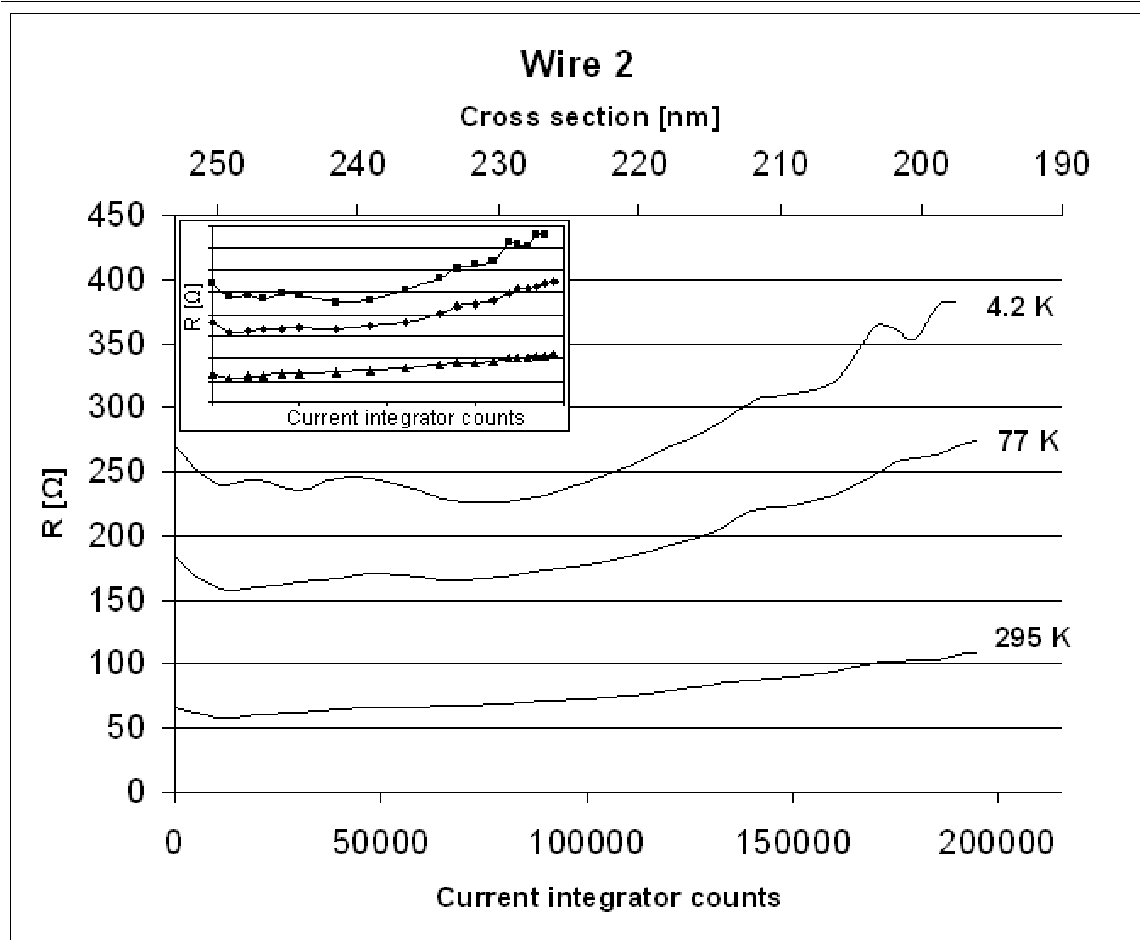

Fig. 4.19: *Evolution of the resistance of wire sample 2. Sample was sputtered 195 000 counts from 45° angle with 0.6 kV acceleration voltage. Initial room temperature resistance was 65 Ω and the last measured room temperature resistance was 107 Ω. Inset shows the measurement data points.*

Initial room temperature resistance of wire sample 3 was 104Ω. Measured series ended after the sample was sputtered 75 100 counts after which the sample broke. Last measured room temperature resistance of the sample was 150 Ω. Sample was sputtered with 0.6 kV acceleration voltage from 45° angle and was rotated randomly during sputtering. This sample showed most dramatic oscillation of the resistance as a function of the cross section of all the studied samples. Measured resistance curves are represented in Fig. 4.21. Largest oscillations occurred between 27 000-37 000 counts of sputtering. That sputtering range is enlarged in the lower picture in Fig. 4.22. Most notable drop

happened at 30 000 counts, when the room temperature resistance was 129 Ω, 77 K resistance was 165 Ω and the 4.2 K resistance almost the same 168 Ω. AC-mode measurement gave the same results in all temperatures after current and voltage probes were interchanged between each other. DC results were 127 Ω, 163 Ω and 166 Ω at 295 K, 77 K and 4.2 K temperatures respectively. Contacts were double checked, they showed normal values and there was no ground connection. In case of a shortcut in the circuit one would expect to see different measurement values of resistance when the current and voltage probes were changed in between and room temperature resistance could also be expected to show some changes. Second similar drop of resistance occurred at 33 000 counts. Then the cooling down was done twice and the sample holder was turned so, that in the later measurement it used four other lines of the dipstick which were in reserve for another sample. Second measurement confirmed the results of the first one. This would rule out a malfunction of dipstick. AC and DC measurements setups had completely different configurations and gave the same results, so the peculiarity was not caused by measuring devices. In the light of all the error checks it must be concluded that the measured oscillation of the resistance is the objective property of the sample. Whether it is caused by QSE, is less certain. Grain boundary in the right side of the sample, which can be seen in Fig. 4.20, could in principle cause some unforeseen changes in resistance, but even then it could be expected to somewhat affect the room temperature resistance as well as the changes in cryogenic resistances are so drastic. There are some unusual changes in the room temperature resistance value later, but in this particular region the room temperature value didn't show any peculiar changes. At 36 000 counts

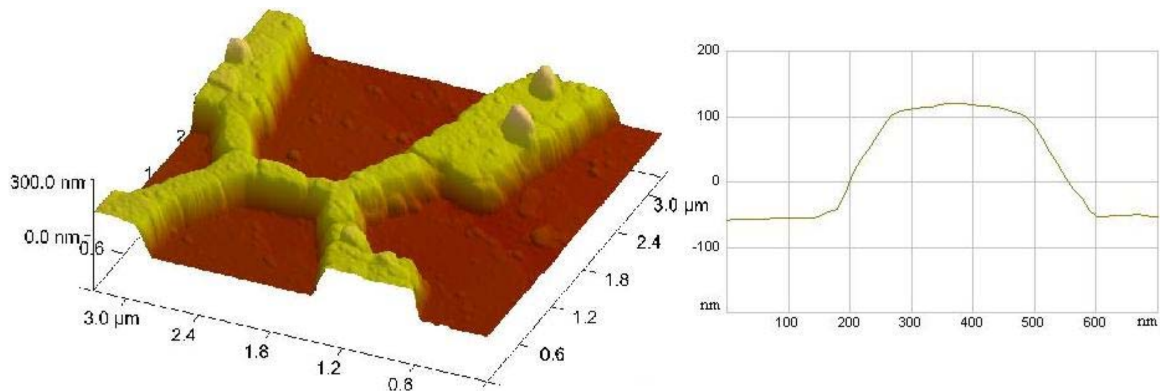

Fig. 4.20: *3D image and the middle cross section profile of wire sample 3 initially.*

of sputtering the cryogenic temperature resistances rises back to 'normal' and then the room temperature resistance drops unexpectedly from 132 Ω to 106 Ω. I can offer no satisfactory explanation for the room temperature resistance drop. AFM image and cross section profile of the wire sample 3 are shown in Fig. 4.20.

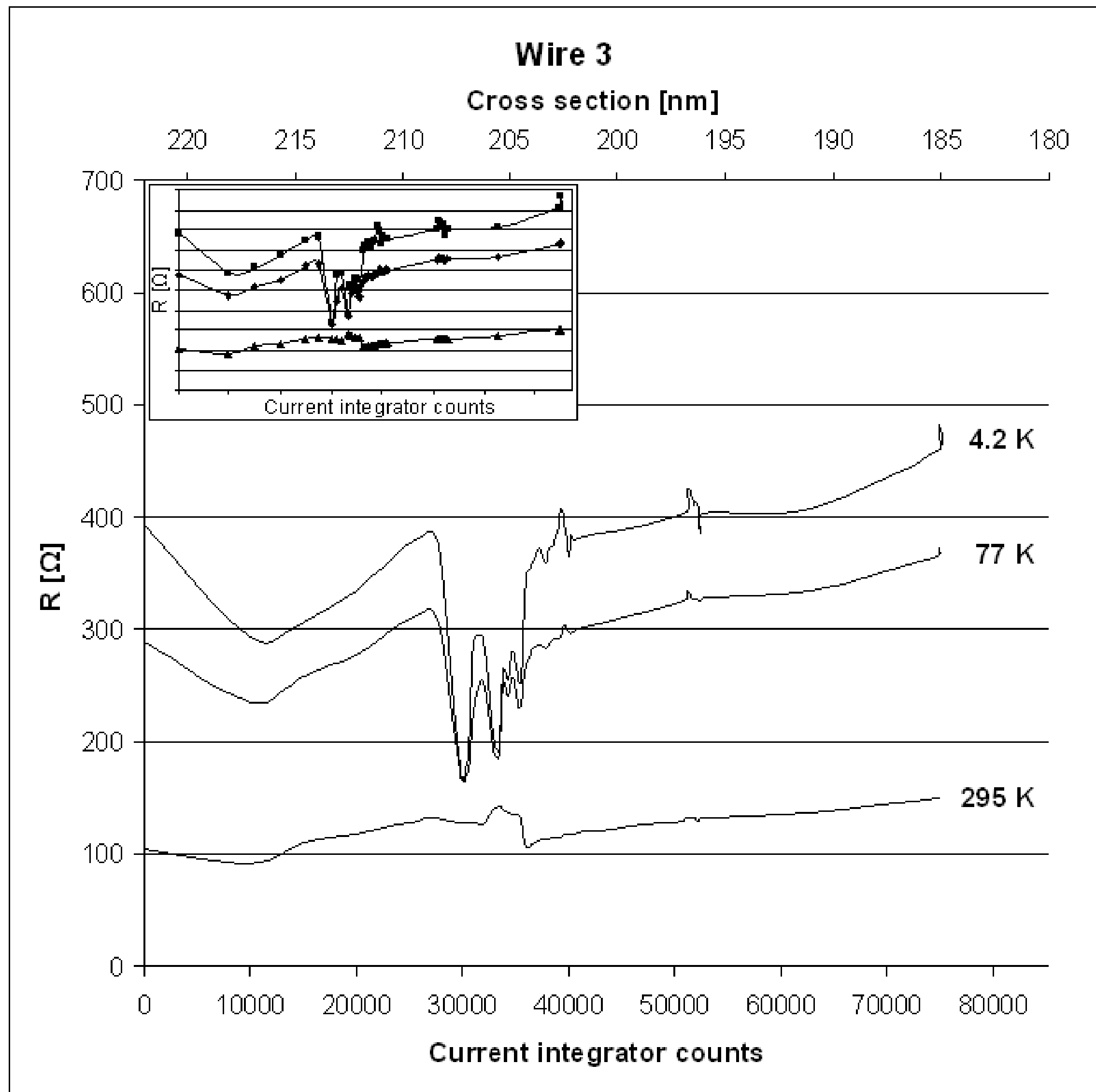

Fig. 4.21: *Evolution of the resistance of wire sample 3. Sample was sputtered 75 100 counts from 45° angle with 0.6 kV acceleration voltage. Initial room temperature resistance was 104 Ω and the last measured room temperature resistance was 150 Ω. Inset shows the measurement data points.*

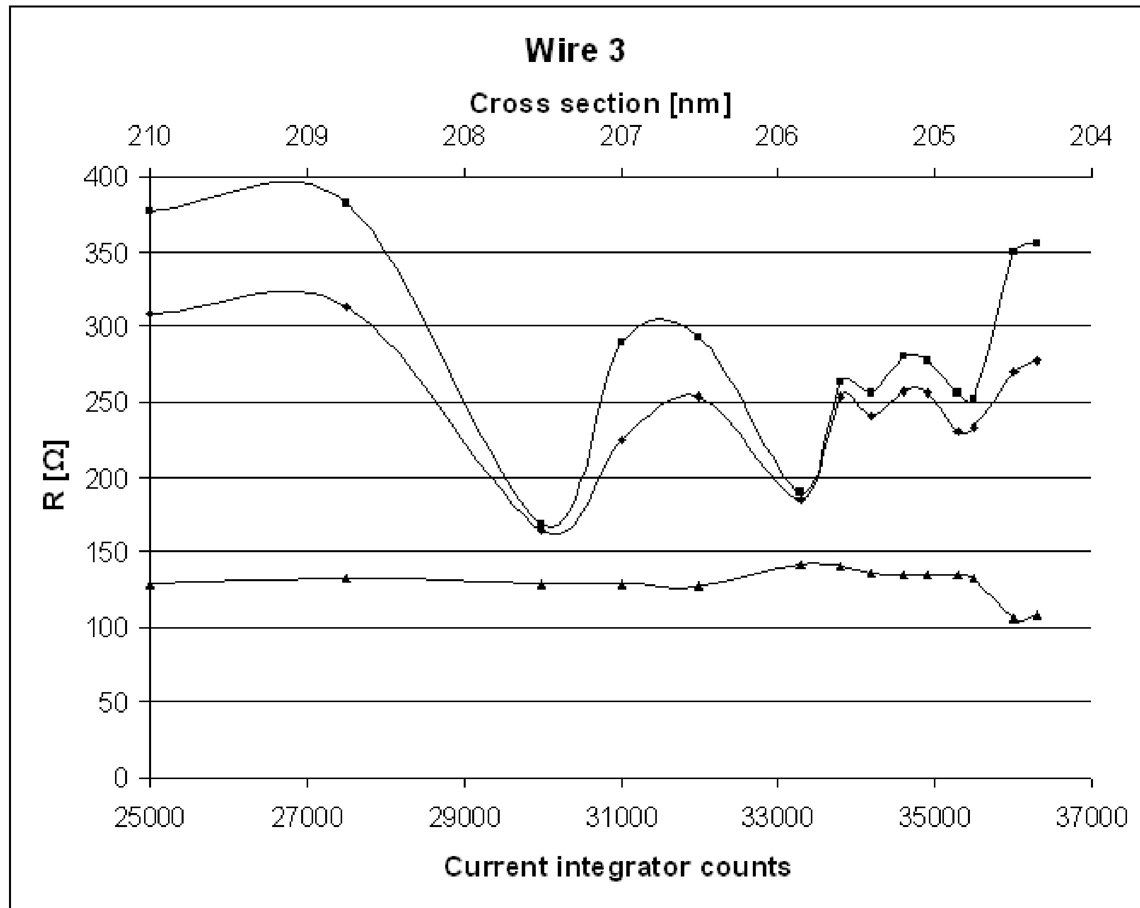

Fig 4.22: *Enlarged picture of the region showing most dramatic oscillation of resistance of wire sample 3 with the data points.*

Initial room temperature resistance of wire sample 4 was 41 Ω. The sample was sputtered first with very small steps with estimated consumption of few atomic layers at the time. Sputtering was done with 0.6 kV acceleration voltage, sputtering angle was 45˚ and sample was rotated randomly during the sputtering. Sample was repaired with re-exposure method when it was sputtered 28 000 counts. Before the repairing process the room temperature resistance was 80 Ω after reparation the value was reduced by 10 % and was 72 Ω. During reparation the sample was spun, aluminum layer was evaporated on top of the resist and finally 200 nm of copper was evaporated on the broken part of the structure. The sample area should have been protected all the time by resist layer, it seems that some metal could have ended on the sample area, but by no means 200 nm

layer of copper, which would have cause much more dramatic changes in resistance. Other possibility is that the crystal structure of bismuth was somehow annihilated or improved when the resist was heated. Resist was heated two times at 160 ˚C, one minute at a time. In any case the later measurement points are not that interesting from the QSE point of view, but show the applicability of the re-exposure method, as the sample broadly speaking holds its properties. In the beginning when sputtering was taken with very small steps, some small oscillation of resistance can be seen at cryogenic temperatures, with the oscillation period of 1 nm or less in cross section. In below the AFM image and the cross section profile of wire sample 4 in Fig. 4.23 and measured evolution of the sample in Fig. 4.24.

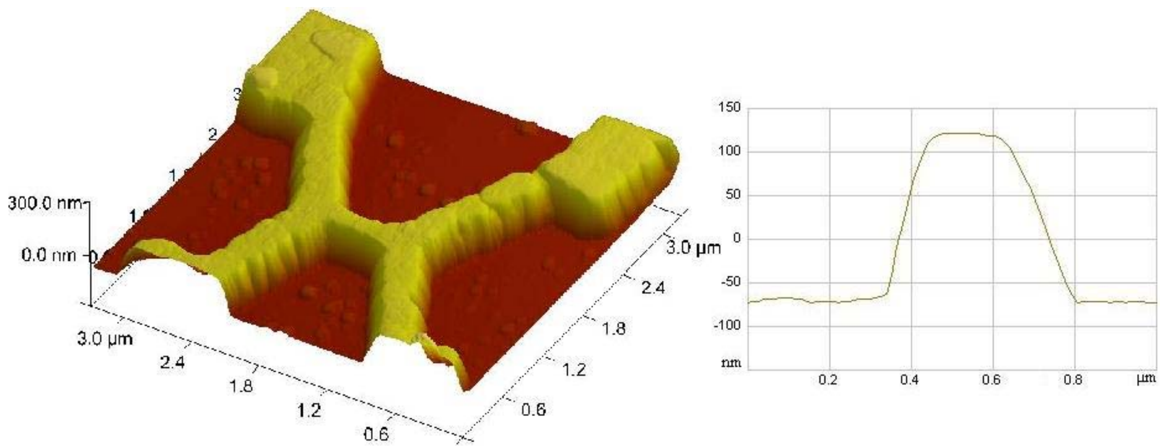

Fig 4.23: *3D AFM picture and the cross section profile of wire sample 4 initially.*

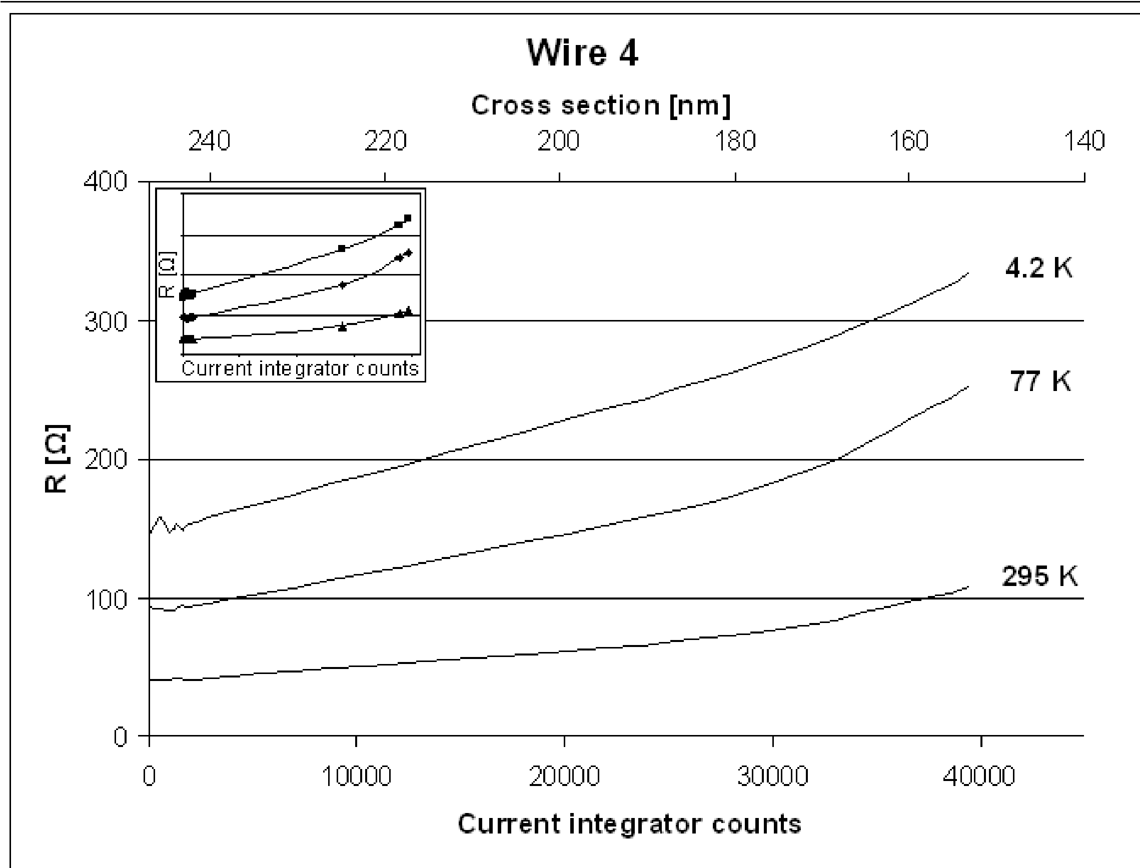

Fig. 4.24: *Evolution of the resistance of wire sample 4. Sample was sputtered 39 500 counts from 45˚ angle with 0.6 kV acceleration voltage. Initial room temperature resistance was 41 Ω and the last measured room temperature resistance was 109 Ω. Inset shows the measurement data points. Contact of this sample was repaired by a re-exposure method at point when the sample was sputtered 28 000 counts by evaporating 200 nm of copper onto the damaged area.*

6 Conclusions

The method of lithographical fabrication of quasi-1-dimensional bismuth nanowires was developed. Ion beam sputtering was used to reduce progressively the cross-sections of the samples enabling the study of a size phenomenon on the same structure eliminating the uncertainty coming from uniqueness of nano-sized samples fabricated in different experimental runs.

Oscillation of resistance as a function of the bismuth nanowire cross-section was observed qualitatively supporting the quantum size effect scenario. However the shape of the oscillations was such that it was difficult to fit results to theoretical model and they are not very consistent with previous experiments. In theory the oscillation should have a periodicity of about 50 nm and an amplitude of tens of percents of the total resistance. In this research the measured amplitude was typically ~2% of the total resistance and the period of a few nanometers of the diameter of the wire or of the thickness of the film. In general the oscillations seem quite arbitrary. Yet the oscillations are only seen at cryogenic temperatures, 77 K curve has generally smaller amplitude than the one measured in 4.2 K, but their local maximuma and minimuma are located at the same points, while the room temperature resistance rose continuously with sputtering as expected.

The discrepancy between our experiments and the theory is associated with the high anisotropy of the energy spectrum of bismuth. Though significant efforts were made to fabricate mono-domain single-crystalline bismuth nanostructures, even in the best samples the nanowire constituted of several crystals of random orientation. Hence electrons with different effective masses contributed to the conductivity resulting in a complicating shape of the corresponding resistance vs. wire diameter dependencies.

Acknowledgments

I would like to thank my mother for all the support during my studies. I would especially like to thank my supervisor Konstantin Arutyuno and doctors Machiec Zigirski and Marko Savolainen with whom I collaborated during my work in the department of physics, and who taught me to operate different scientific instruments and with whom I had inspiring discussions about physical issues. In general I would also like thank all the people of our research group, the Nanoscience Center and the Department of Physics.

References

[1] S. Farhangfar, Phys. Rew B 74, 205318 (2006)

[2] A. I. Il'in, L. I. Aparshina, and B. N. Tolkunov, Russian Microelectronics, Vol. 32, No 6, (2003)

[3] S. Farhangfar, Phys. Rew. B 76, 205437 (2007)

[4] V. N. Lutskii, Phys. Stat. Sol. (a) 1, 199, (1970)

[5] S. Colin, Phys. Rev. 166,643, (1969)

[6] Z. Zhang, X. Sun, M.S. Dresselhaus, Phys. Rev. B, Vol. 61, No 7, (2000).

[7] V. B. Sandomirskii, Soviet Physics JETP, Vol. 25, No 1, (1967)

[8] M. S. Dresselhaus, E. I. Rogacheva, S. N. Grigorov, O. N. Nashckekina, and S. Lyubchenko, Appl. Phys. Lett. Vol. 82, No 16, (2003)

[9] S. B. Corin. PhD thesis, Electric properties of Bi nanowires, MIT, 2002.

[10] Yu. F. Komnik, E. I. Bukhshtab, Yu. V. Nikitin, and V. V. Anrievskii, Soviet Physics JETP, Vol. 33, No 2, (1971)

[11] Yu. F. Komnik and E. J. Bukhstab, JETP LETT. 6, 58 (1967).

[12] J. Heremans, C. M. Thrush, Y.-M. Lin, S. Corin, Z. Zhang, M. S. Dressehaus, and J. F. Mansfield, Phys. Rev. B, Vol. 61, No 4, (2000)

[13] M. Savolainen, V. Touboltsev, P. Koppinen, K.-P. Riikonen, and K. Yu. Arutyunov, Appl. Phys. A 79, 1769-1773,(2004).

[14] M. Zgirski, K.-P. Riikonen, V. Touboltsev, and K. Yu. Arutyunov, Nano Lett. Vol. 5, No. 6, 1029-1033, (2005)

[15] M. Zgirski PhD thesis, Experimental study of fluctuations in ultranarrow superconducting nanowires, University of Jyväskylä, (2008).

[16] M. Savolainen PhD thesis, Size sensitive phenomena in superconducting wires and single charge devices, University of Jyväskylä, (2004).

[17] K. Yu. Arutyunov, M. Zgirski, K.-P. Riikonen, and P. Jalkanen, I.RE.PHY, Vol. 1, No. 1, (2007)

[18] M. Zgirski, K.-P. Riikonen, V. Touboltsev, P. Jalkanen, T. T. Hongisto, and K. Yu. Arutyunov, Nanotechnology, 19, 055301, (2008)

[19] O. Wada, J.Phys. D: Appl.Phys., Vol. 17, 2429-2437, (1984)

[20] L.C. Chao, C.C. Liau, J.W. Lee and F.C. Tsai, J. Vac. Sci. Technol. B. Vol. 25, Issue 6, 2168-2170, (2007).

[21] G. Carter, M. J. Nobes and J. L. Whitton, Appl. Phys. A 38, 77-95, (1985).

[22] Generalic, Eni. "Bismuth." *EniG. Periodic Table of the Elements*. 31 Mar. 2008. KTF-Split. (Accessed 5 Feb 2009). http://www.periodni.com/en/bi.html

[23] J.F. Ziegler, J.P. Biersack, M.D. Ziegler, the Stopping and Range of Ions in Matter (SRIM), freeware (Accessed Feb 4 2009). www.srim.org

List of publications contributed by author

1. M. Savolainen, V. Touboltsev, P. Koppinen, **K.-P. Riikonen** and K. Yu. Arutyunov, "Ion beam sputtering method for progressive reduction of nanostructures dimensions", **Appl. Phys. A** 79, 1769-1773, (2004).

2. M. Zgirski, **K.-P. Riikonen**, V. Touboltsev, and K. Arutyunov "Size Dependent Breakdown of Superconductivity in Ultranarrow Nanowires", **Nano Letters**, 5, 1029 (2005).

3. K. Arutyunov, M. Zgirski, **K.-P. Riikonen**, and P. Jalkanen, "Quantum Limitations of Electron Transport in Ultra-Narrow Nanowires", (invited review article) **International Review of Physics** (IREPHY), V. 1, N1, pp. 28-30, (2007).

4. M.Zgirski, **K-P. Riikonen**, V. Tuboltsev, P. Jalkanen, T. T. Hongisto and K. Yu. Arutyunov, "Ion beam shaping and downsizing of nanostructures", **Nanotechnology** 19 055301-1 - 055301-6 (2008).

5. M. Zgirski, **K.-P. Riikonen**, V. Touboltsev and K.Yu. Arutyunov, "Quantum fluctuations in ultranarrow superconducting nanowires", **Phys. Rev. B**. 77, 054508-1 - 054508-6 (2008).